

NASA TECHNICAL NOTE



NASA TN D-4889

2.1

0131571



TECH LIBRARY KAFB, NM

NASA TN D-4889

LOAN COPY: RETURN TO  
AFWL (WLIL-2)  
KIRTLAND AFB, N MEX

# CALORIMETRIC, OPTICAL, AND VIBRATION INVESTIGATIONS OF STRETCH-FORMED ALUMINUM SOLAR CONCENTRATORS

*by Marvin D. Rhodes and Conrad M. Willis*

*Langley Research Center*

*Langley Station, Hampton, Va.*



0131571

CALORIMETRIC, OPTICAL, AND VIBRATION INVESTIGATIONS OF  
STRETCH-FORMED ALUMINUM SOLAR CONCENTRATORS

By Marvin D. Rhodes and Conrad M. Willis

Langley Research Center  
Langley Station, Hampton, Va.

NATIONAL AERONAUTICS AND SPACE ADMINISTRATION

---

For sale by the Clearinghouse for Federal Scientific and Technical Information  
Springfield, Virginia 22151 - CFSTI price \$3.00

# CALORIMETRIC, OPTICAL, AND VIBRATION INVESTIGATIONS OF STRETCH-FORMED ALUMINUM SOLAR CONCENTRATORS

By Marvin D. Rhodes and Conrad M. Willis  
Langley Research Center

## SUMMARY

Three stretch-formed aluminum solar concentrators were evaluated in this investigation. The models represent three phases of a research and development program and all were 1.52-m-diameter paraboloids with a nominal rim angle of  $\pi/3$  rad. Calorimetric tests were made on each model to determine the improvement in model performance caused by changes in model design and fabrication. Model 3 was superior to the other models in both geometrical accuracy and specular reflectance and is considered suitable for thermionic applications.

Optical-ray-trace tests were performed on models 1 and 2 to determine the magnitude and location of surface slope errors. The largest slope errors occurred near the gore seams but the region of high error was only about 8 percent of the total area. Ray-trace data were also used to calculate geometric efficiency by three methods. Only the random error method gave reasonable results for both models.

Vibration tests on model 1 caused failure in the welds of the rim support ring structure but subsequent calorimetric tests revealed little or no reduction in concentrator efficiency.

## INTRODUCTION

Studies of space power systems have indicated that solar thermionic systems are resistant to radiation damage and are capable of operating in a high-temperature environment (ref. 1). Since the thermionic convertor requires temperatures of about 2000° K (ref. 2) for efficient operation, the solar concentrator must have good geometrical accuracy and high specular reflectance. Concentrators which are capable of achieving this goal have been fabricated of electroformed nickel (ref. 3) and investigations of one of these concentrators are reported in references 4 and 5. Nickel concentrators, however, may interfere with magnetically sensitive instruments, such as the magnetometers, used on some spacecraft.

In an effort to circumvent the problem of magnetic interference, other materials have been investigated for the fabrication of solar concentrators. Aluminum is one such material, and in addition to its nonmagnetic property it also makes possible the use of a considerably thinner shell (ref. 6) than is required with nickel. Since aluminum is less dense than nickel the concentrator will also have a lower mass. One of the fabrication techniques that appeared practical for obtaining aluminum concentrators was to form them by stretching flat sheets over a paraboloidal die. Therefore, a three-phase stretch-forming development program (refs. 6, 7, and 8) was conducted to determine the feasibility of fabricating efficient stretch-formed solar concentrators. At least one model was constructed during each phase and a preliminary evaluation made to indicate the areas of possible improvement before starting the next phase. The object of the present study was to investigate three 1.52-m-diameter paraboloidal stretch-formed solar concentrators and to evaluate their possible use with thermionic convertors. Each model represents one phase of the development program and the third phase model is considered representative of the state of the art for this type concentrator.

The investigation reported herein consists of calorimetric tests of all models, optical tests on two models, and vibration tests on one model. The calorimetric tests were performed in sunlight using a water-cooled-cavity calorimeter with aperture diameters ranging from 1.56 to 8.34 solar-image diameters. The optical tests consisted of directing a collimated beam of light parallel to the optical axis and intercepting the reflected beam with a focal-plane image plate. The image displacements from the optical axis were used to calculate the deviation of concentrator slope from that of a perfect paraboloid. The optical data were also used to calculate approximate concentrator efficiency. Vibration tests were made on one of the models to determine its resonant frequencies and its ability to withstand loads simulating a launch vibration environment. Calorimetric tests were repeated after vibration tests to determine any change in concentrator efficiency.

## SYMBOLS

The units used for the physical quantities defined in this paper are given in the International System of Units (SI). Factors relating this system to U.S. Customary Units are presented in reference 9.

$f$	nominal design focal length, centimeters
$f_a$	distance from concentrator vertex plane to calorimeter aperture or from vertex plane to ray-trace image plate, centimeters (see fig. 9)

$g$	acceleration of gravity, 9.82 meters per second <sup>2</sup>
$h$	distance from point on concentrator surface to plane of image plate, $f_a - \frac{r^2}{4f_a}$ , centimeters (see fig. 9)
$i,j,k$	axes for rectangular Cartesian coordinates; origin is on surface of design paraboloid, k-axis lies along paraboloid normal, and j-axis intersects optical axis (see fig. 9)
$R_a$	radius of calorimeter aperture, centimeters
$R_i$	calculated radius of solar image formed at focus by cone of rays reflected from paraboloid vertex, $f \tan \alpha$ , centimeters
$R_s$	radius of solar concentrator, centimeters
$r$	test radius, distance from concentrator axis to collimated light, centimeters
$S_p$	projected area of solar concentrator, $\pi R_s^2$ , centimeters <sup>2</sup>
$S_t$	partial area assigned to a set of test data, centimeters <sup>2</sup>
$S_u$	unobscured concentrator area, $S_p$ minus Projected area that is shaded by calorimeter and its supports, centimeters <sup>2</sup>
$\Delta T$	temperature increase of water flowing through calorimeter, K <sup>o</sup>
$w$	mass-flow rate of calorimeter water, kilograms per second
$x,y,z$	rectangular Cartesian coordinates with system origin at focal point, $z$ is measured along concentrator axis, centimeters (see fig. 9)
$\alpha$	half-angle subtended by sun, 4.6 milliradians
$\beta$	misorientation angle, angle between concentrator axis and solar rays, milliradians
$\gamma$	measured solar irradiance on unit area normal to rays, watts per meter <sup>2</sup>

$\delta_c$	circumferential error in slope of reflective surface, angle between paraboloid normal and projection of concentrator normal on ik plane (fig. 9(b)), milliradians
$\delta_r$	radial error in slope of reflective surface, angle between paraboloid normal and projection of concentrator normal on jk plane (fig. 9(b)), milliradians
$\bar{\delta}_c, \bar{\delta}_r$	mean value of slope error, milliradians
$\eta$	calorimetric efficiency, ratio of energy absorbed by calorimeter water to energy incident on concentrator, $\frac{4.183 \times 10^7 w \Delta T}{\gamma S_u}$
$\eta_g$	geometric efficiency calculated from ray-trace data, ratio of energy entering a given size focal-plane aperture to energy specularly reflected from concentrator
$\eta_{g,m}$	geometric efficiency measured by calorimetric tests, $\eta/\rho$
$\rho$	specular reflectance of concentrator surface
$\sigma$	standard deviation of circumferential or radial component of slope error from mean error, $\left[ \frac{\sum \delta^2 - \frac{1}{N} (\sum \delta)^2}{N - 1} \right]^{1/2}$ where $\delta$ represents either $\delta_c$ or $\delta_r$ and N is number of data points
$\phi$	azimuth angle, measured in plane normal to concentrator axis and used to locate points on concentrator, radians (see fig. 9)

## MODELS

Three stretch-formed aluminum paraboloidal solar concentrators were investigated. The models were about 1.52 m in diameter with a nominal rim angle of  $\pi/3$  rad. Sketches of each model are presented as figure 1 and photographs of model 2 are shown as figure 2. The concentrator shells were formed by stretching sheets of aluminum alloy over a paraboloidal male die. After stretch-forming, the aluminum sheets received a surface improvement coating of thinned epoxy, a buffer coating of silicon oxide, and a reflective coating of vacuum-deposited aluminum. Two  $\pi/4$ -rad sectors were then cut from each stretched sheet and eight sectors were assembled on the die

now used as a jig. The sectors were joined by overlap strips cut from stretched stock and bonded to the back surface. The concentrator was vacuum bagged to hold it against the die until the epoxy bonds had cured. A rim support ring containing three mounting brackets was bonded to the back surface of the concentrator before removing it from the die. The master die, which was an accurate glass searchlight mirror, was used directly in fabricating models 2 and 3 and an epoxy replica of the master die was used for model 1.

### Model 1

The shell material for model 1 was 0.041-cm-thick sheets of 5052-O aluminum alloy. This material was chosen because it is a work hardening alloy and is therefore less susceptible to age hardening which may result in contour changes. In addition, it can be supplied in large widths with a surface finish less than 30 nm rms. One disadvantage in this material which became apparent during stretch-forming was that it developed strain lines which could not be completely covered by the surface improvement coating. The sheets were stretched over a reinforced epoxy replica of the glass master die. The replica was made in a two-step process and the surface had defects not present in the master. The thinned-epoxy surface improvement coating was applied by a dip coating process. This technique left small runs and bubbles in the surface which reduced the reflectivity of the subsequent vacuum-deposited aluminum (ref. 6). The aluminum reflective surface received a protective overcoating of silicon oxide. The sectors were bonded together with 2.5-cm-wide overlap strips. A rim support ring was fabricated from sheets of aluminum alloy and was rectangular in cross section (fig. 1(a)). Total concentrator mass (rim support plus shell) was 5.1 kg. The shell mass was estimated to be 2.2 kg in reference 6. (Model 1 is called S/N 2 in ref. 6.) Reference 6 also contains additional model details.

### Model 2

The shell material for model 2 was 0.043-cm-thick sheets of 3003-O aluminum alloy. This material was selected because it did not develop the undesirable strain lines associated with stretching the model 1 material. The 3003-O alloy also had a surface finish which was less than 30 nm rms. The difference in thickness in the sheets for the two models was incidental and is not believed to have had any effect on concentrator accuracy. The aluminum sheets were stretched over the glass master die instead of a replica of the die as was done for model 1. Surface improvement coatings received a great deal of effort during this phase of the study and a spray process was developed that gave a uniform coating. However, the formulation selected for use failed to completely fill the grainy surface and may have caused an increase in the diffuse reflectance of the surface. The reflective surface had a protective overcoating of silicon oxide. The

silicon oxide coating was not uniform and may have further lowered the specular reflectance of the surface. The stretched sectors were bonded together with 2.5-cm-wide overlap strips. A preliminary investigation of this model reported in reference 7 indicated that the sector edges have surface errors larger than the general level of error in the concentrator. The rim support ring for this model was formed of two sections bonded together (fig. 1(b)). Shell mass was estimated to be 2.5 kg (ref. 7) and total concentrator mass was 5.3 kg. Additional details can be found in reference 7.

### Model 3

The shell of model 3 was made from 0.041-cm-thick sheets of 3003-O aluminum alloy similar to that used for model 2. The glass master was used as the stretch-forming die and new positioning techniques were incorporated so that the stretched sheets could be accurately positioned during trimming and assembly. The surface improvement coating used during this phase was superior to that used on model 2 and was sufficient to cover the grainy surface of the stretched sheets. No protective overcoating was used on this concentrator as had been used on the two previous models. A new trimming guide was developed and used to reduce trimming distortion of the joints. In addition, a new sector joint design was incorporated. The sectors were joined by two overlap strips 3.8 and 1.9 cm wide (fig. 1(c)). The rim support ring for this model was an aluminum torus which was attached to the shell with an aluminum skirt. The aluminum skirt was used because tests on several rim support ring configurations indicated this design introduced less surface distortion than other techniques. The mass of the concentrator shell was estimated to be 2.5 kg (ref. 8) and the total mass was 4.9 kg. Fabrication procedure and additional details can be found in reference 8.

## APPARATUS AND TESTS

### Calorimetric

The calorimetric investigations were performed in sunlight utilizing the solar tracker shown in figure 3. The tracker automatically maintained any preset alignment of the concentrator axis with the solar rays. A water-cooled-cavity calorimeter located in the focal region was equipped with various sized aperture plates.

Tests were performed to determine the effect of aperture size, the effect of mislocation of the calorimeter along and transverse to the optical axis, and the effect of misorientation of the optical axis with the sun. The ranges of test variables were calorimeter aperture sizes from  $1.56R_i$  to  $8.34R_i$ , axial calorimeter movement of  $0.06f$ , transverse calorimeter movement of  $\pm 4R_i$ , misalignment of the optical axis with the solar rays of  $\pm 30$  mrad. A more complete description of the apparatus and test techniques can be found in reference 4.

### Optical Ray Trace

The test fixture shown in figure 4 was used to perform optical-ray-trace tests on models 1 and 2. A narrow beam of collimated light parallel to the concentrator axis was reflected to a focal-plane image plate and the image location was recorded photographically. The concentrator was divided into 720 equal areas and data were taken at the center of each area. Additional data were obtained near the seams and torus to evaluate their effect on the reflective surface. Detailed information on the test apparatus and techniques can be found in reference 5.

### Vibration

Model 1 only was evaluated for the vibration portion of the investigation. The resonant frequencies and nodal patterns of the concentrator were determined by using an air jet vibration exciter. The test setup is shown in figure 5. The concentrator was suspended from a cantilever truss by small cables and the exciter was mounted about 3 cm above the concentrator rear surface. The vibration exciter is of the type described in reference 10 and consists of an air jet which is interrupted periodically by a notched rotating disk. Concentrator response was measured by a velocity-type vibration transducer. The transducer was mounted on a counterbalanced arm attached to a movable stand, to permit examination of any desired point on the concentrator. At each resonant frequency the vibration transducer was moved about the concentrator to determine the nodal patterns. This procedure was repeated for several exciter locations.

The electrodynamic vibration exciter shown in figure 6 was used for simulation of a launch vibration spectrum. This exciter is a commercial model having sine- and random-wave generators and a force capability of 125 kN (1 kilonewton (kN) = 224.8 lbf). For the transverse excitation used in this investigation, the exciter armature was attached to a large aluminum plate floating on an oil film between the plate and a large granite block. A block of laminated plywood was bolted to the aluminum plate. The concentrator was supported by attaching its mounting brackets to heavy aluminum standoff mounts which were fastened to the top of the plywood block. Response of the concentrator was determined by using small accelerometers having a mass of about 0.017 kg and a response range of 3 to 6500 Hz. These accelerometers were mounted on small plastic blocks attached to the concentrator shell at approximately  $\pi/3$ -rad intervals as indicated in figure 7. They could be oriented to measure acceleration along either the concentrator axis or a radial axis. A shielded mutual inductance coil was mounted on the plywood block to measure axial deflection of the concentrator vertex. Both the accelerometer and coil outputs were recorded by an optical oscillograph. The launch simulation vibration spectrum used for flight qualifications tests is shown in table 1(a). These specifications are similar to those used in previous investigations (refs. 11 and 12). Test conditions for each run are listed in table 1(b).

## ACCURACY

The calorimetric efficiency  $\eta$  is considered accurate to within  $\pm 0.02$  based on instrument component errors and repeatability of data. The image coordinates  $x$  and  $y$ , measured during the optical test, were used to calculate slope errors  $\delta_c$  and  $\delta_r$ . The  $x$  and  $y$  coordinates were measured to within  $\pm 0.02$  cm, which produced an uncertainty in slope errors  $\delta_c$  and  $\delta_r$  dependent upon the test radius, and varied from  $\pm 0.15$  mrad for both at the vertex to  $\pm 0.13$  mrad for  $\delta_c$  and  $\pm 0.06$  mrad for  $\delta_r$  at the rim. The data were analyzed for error due to misalignment of the concentrator axis with the turntable axis of rotation. This effect was considered insignificant; consequently, no correction was made.

The electrodynamic vibration exciter was controlled by a servo system which generally kept the input acceleration level to the concentrator to within  $\pm 12$  percent of the prescribed level. The accelerometers and recording system used during this part of the investigation were calibrated to within  $\pm 0.4g$ . The largest value of axial shell deflection is considered accurate to within  $\pm 0.01$  cm.

## RESULTS AND DISCUSSION

### Calorimetric

A calorimetric exploration of the concentrator focal region was made to determine the aperture location producing maximum efficiency. Surveys were then made along axial and transverse axes to determine the effect of calorimeter location. Orientation surveys were also made to determine the effect of misalignment of the concentrator axis with the solar rays.

Axial surveys.- The variation in calorimetric efficiency with axial location  $f_a$  of the heat receiver aperture is shown for each concentrator at several aperture sizes in figure 8(a). The aperture location was normalized by the nominal focal length (66 cm) of the master die. The focal length, as indicated by maximum efficiency, was about  $0.99f$  (65.3 cm) for all three concentrators. It is not known whether this apparent change in focal length between die and concentrator was due to use of an erroneous nominal value or an actual change during concentrator fabrication. The agreement in focal length of all three concentrators is within the  $\pm 0.10$  cm estimated measurement accuracy for this dimension. This agreement indicates that the master die (used to stretch models 2 and 3) and its replica (used to stretch model 1) had the same focal length even though the replica had errors not present in the master. It should also be noted that each of the models has approximately the same focal length for every aperture tested; this indicates that the models have a surface approximating a paraboloid.

Transverse surveys.- The variation in calorimetric efficiency with lateral location of the calorimeter is presented in figure 8(b). Maximum efficiency occurred at about the same lateral position for all aperture sizes. Preliminary searches along the other orthogonal lateral axis produced results similar to those shown in the figure; therefore, the energy distributions were symmetrical with respect to the optical axis.

Orientation surveys.- The variation in calorimetric efficiency with misorientation of the concentrator axis with the solar rays is presented in figure 8(c) for models 1 and 2. At aperture ratios  $R_a/R_i$  of 2 to 3, suitable for thermionic convertors, the efficiency decreases rapidly with misorientation; therefore, accurate orientation is required to maintain high efficiency.

The flatter efficiency curves (fig. 8(c)) of model 2 for large aperture sizes near  $\beta = 0$  indicate that its focal-plane energy distribution is smaller than that for model 1.

A perfect concentrator with the same  $\pi/3$ -rad rim angle would have constant efficiency with small misorientations for all aperture radii larger than  $2.7R_i$ , the radius of the solar energy distribution from the entire concentrator.

Aperture size.- A comparison of the performance of the three models is shown in figure 8(d) by presenting the maximum value of efficiency at each test aperture size. Also shown in the figure for comparison is the performance of a  $\pi/3$ -rad rim angle concentrator with perfect geometry and a specular reflectance equal to that of model 3. At an aperture ratio of 2.5 which is in the range of interest for use with thermionic converters, model 3 has the best performance with an efficiency of 0.85 which is only about 0.05 less than a concentrator with perfect geometry. At this aperture size the results of improvements incorporated in models 2 and 3 are readily apparent and a significant increase in efficiency of 0.30 is noted between models 1 and 3. Note that model 3 attains maximum efficiency at a smaller aperture size than the other models and therefore must have the best geometrical accuracy. However, the geometry can be better compared by optical data and only the differences due to reflectance are discussed in connection with this figure. All curves are nearly flat at the larger aperture ratios; this indicates that nearly all the specularly reflected energy is entering the heat receiver. Since reradiation losses were small at the water-cooled-calorimeter temperatures, the maximum efficiency is therefore considered equal to the specular reflectance. Model 3 had the highest value of specular reflectance which was about 0.905. Slightly lower reflectance values of about 0.89 were obtained from spectrophotometric measurements on flattened samples of the model 3 stretched panels and this value agrees with results reported in reference 8. However the reflectance inferred from the calorimetric data agrees with the spectrophotometric values within the estimated experimental accuracy. The high specular reflectance of model 3 is believed due to the use of a better surface improvement coating and the absence of a protective overcoat. Model 2 had the lowest

value of specular reflectance; this is believed due to the failure of the surface improvement coating to fill adequately the grainy surface of the stretched sheets and a protective overcoating of poor optical quality (ref. 7).

### Optical

Optical-ray-trace tests were performed to determine the magnitude and location of surface slope errors. Once the location of these errors is known, it may be possible to assign the cause of the error to a specific feature such as the rim support ring or sector seams. Models 1 and 2 were tested during this investigation and the data for model 2 showed good agreement with published data obtained by the model fabricator. The model fabricator had also published data for model 3 and these results are shown herein for comparison with models 1 and 2.

Image displacements.- The basic data for the optical part of this investigation were the  $x$  and  $y$  coordinates specifying the displacement of focal-plane images from the concentrator axis. The coordinate systems used for these measurements are shown in figure 9. It can be seen from figure 9(a) that the  $x$  and  $y$  components of the image displacement are affected by the image-plate distance setting  $f_a$ . The setting was selected by making preliminary surveys at several settings near the focus and by using the value of  $f_a$  that resulted in a minimum variation for the  $y$  component of image displacement with radial movement of the collimator. Ideally the image plate distance should be equal to the aperture distance that produced maximum efficiency during calorimetric tests, and for each model the difference in the two values was within the accuracy of measurement. Some typical test data for models 1 and 2 are shown in figure 10. The  $x$  and  $y$  coordinates are shown as a function of angular location for test radii at  $0.25R_s$  and  $0.97R_s$ . In general, the variation with angular location is of a random nature and this tends to obscure the variation between models. However, the rms value of image displacement from the optical axis was 1.0 cm for the model 1 data and only 0.3 cm for the model 2 data.

Slope errors.- The slope errors in the concentrator surface were calculated from the  $x$  and  $y$  coordinates of image displacement by using the formulas shown in figure 9(b). These errors were calculated by assuming that all image displacements result from a rotation of the reflective surface; displacements of the concentrator from an ideal paraboloid were neglected. Therefore, the slope errors calculated by the formulas shown in figure 9(b) do not necessarily represent the actual concentrator imperfections but an equivalent set of errors that would produce the given focal-plane image displacements. The radial and circumferential error components  $\delta_r$  and  $\delta_c$  represent the angles between the paraboloid normal and the projection of the concentrator normal on planes defined by the paraboloid normal and the  $i$  or  $j$  axis. A tabulation of the mean

error  $\bar{\delta}$  and standard deviation  $\sigma$  of models 1 and 2 as determined in the present investigation is shown in the following table:

Source	Model 1				Model 2				Model 3			
	$\delta_r$		$\delta_c$		$\delta_r$		$\delta_c$		$\delta_r$		$\delta_c$	
	$\bar{\delta}_r$	$\sigma$	$\bar{\delta}_c$	$\sigma$	$\bar{\delta}_r$	$\sigma$	$\bar{\delta}_c$	$\sigma$	$\bar{\delta}_r$	$\sigma$	$\bar{\delta}_c$	$\sigma$
	0.73	3.03	0.01	3.08	0.24	0.86	0	1.71				
Present investigation												
Reference 8					.24	.83	.12	1.10	0.13	0.46	0.15	0.61

Also shown in the table are the same statistical parameters for models 2 and 3 as reported in reference 8. The investigation reported in reference 8 used a different ray-tracing technique (the projected grid method) from the one employed in this study. However, a comparison of the results of both methods for model 2 shows good agreement. The circumferential components do not agree quite as closely as the radial components. This is probably due to a difference in the reduction of data rather than a difference in test techniques. The data for the investigation reported herein were reduced in such a manner that the average circumferential error was made zero because the concentrator surface at any test radius forms a closed curve. The improvement in geometry in successive models as first observed from calorimetric tests is substantiated by the optical tests. The standard deviation of both error components decreased by a factor of approximately 2 from model 1 to 2, and an equivalent decrease was noted from model 2 to 3.

Figure 11 presents the fraction of concentrator area having slope errors less than a specified value. The data for model 3 were obtained from reference 8 and do not include 6.5 percent of the concentrator projected area because it had errors too large to measure by the projected grid method. Each model shows a significant improvement over the previously fabricated model in both radial and circumferential error components. The improved geometrical accuracy of model 2 over model 1 has been attributed to stretch-forming over a more accurate die and the use of a material having superior plastic strain properties (ref. 7). Reference 8 attributes part of the improvement in geometry between models 2 and 3 to improvements in seam design and trimming methods. Other differences (ref. 8) between models 2 and 3 which may have improved the geometry were a reduction in the airborne dust deposited on the aluminum stock during stretch-forming operations, the use of pilot holes for accurate location of the stretched panels, and a different rim support ring design.

During the present investigation data were taken in the vicinity of the seams on model 2 to determine the amount of seam distortion and the area affected. Figure 12 presents slope error as a function of distance from the sector seam for two test radii,

one of which ( $0.97R_g$ ) lies within the area of contact between the shell and rim support ring. Slope errors were larger near the sector seams with the largest error occurring in the vicinity of the sector seam intersection with the rim support ring. However, in every case the distortion was confined to an area about the width of the overlap strip. Since the overlap strips cover only about 8 percent of the total area, the loss in concentrator efficiency is small. The data also indicate that the panel edges deflect outward from the concentrator axis. Reference 7 states that this outward deflection results from overcompensation during assembly for a deflection in the opposite direction due to trimming. Shrinkage of the adhesive used to bond the seam overlap strips to the concentrator rear surface also contributed to the poor geometry near the seams (ref. 7). The data presented in reference 8 show that a redesign of the sector seam, which was incorporated in model 3, reduced the slope error near the seam.

Geometric efficiency.- Concentrator geometric efficiency was calculated from optical-ray-trace data by three methods for models 1 and 2. The methods used are approximations and are generally less accurate than calorimetric tests. However, they offer some advantage because they require less elaborate test equipment and are not subject to delay by unfavorable weather. Even though high accuracy might be required at the design point, the calculated efficiency might still be useful for determining trends at off-design conditions and, thus, greatly reduce the calorimetric testing required to evaluate a concentrator.

The methods used during this investigation were image count (ref. 5), uniform image (ref. 5), and random error (ref. 13). The image count method is the simplest procedure and consists of taking the ratio of the number of ray-trace images falling inside a circular aperture to the total number of images. The uniform image method was developed by assuming the solar image to be a circle with a diameter equal to the minor axis of the actual elliptical image. The solar image was also assumed to have a uniform energy distribution and the efficiency was calculated by taking the average ratio of image area inside the aperture to the total image area for all the data considered. For the random error method, the surface slope error is assumed to be randomly distributed about a mean value of zero and the only information required is the physical dimensions of the concentrator and the standard deviation of the surface slope error components.

The difference between calculated and measured geometric efficiency as a function of aperture ratio is shown in figure 13 for models 1 and 2. The measured geometric efficiency was determined by dividing the calorimetric efficiency shown in figure 8(d) by the specular reflectance. In the region of interest for use with thermionic converters (aperture ratios of 2 to 3) all methods had errors less than 0.05 for model 1. However, for model 2 which had a much higher calorimetric efficiency in the region of interest, the results of the random error method were closest to the measured data, but even with this

method the maximum error in efficiency was slightly greater than 0.07. This error may be due to the failure of the data to meet the assumed condition of a normal distribution about a mean value of zero.

A comparison of the data with a normal distribution is made in figure 14. The percentage of slope errors less than a given value are plotted as a function of standard deviation  $\sigma$  from the mean; and the normal distribution appears as a straight line. The value of a standard deviation and the mean value are also listed in the figure. The circumferential component of slope error for model 1 (fig. 14(a)) is very close to the normal distribution but the radial component is significantly different. Both components of slope error for model 2 (fig. 14(b)) showed considerable deviation from the normal distribution.

The errors in predicted efficiency by the other two methods also probably result from the distribution of the data. The efficiency was correctly calculated by using both the uniform image and point count methods for those data points representing solar images that do not intersect the aperture edge. The approximations made in calculating the efficiency for an intersecting image may introduce a large error, however images having centers inside the aperture tend to produce errors opposite in sign to those with centers outside the aperture. Consequently, the error in concentrator efficiency will be partially dependent upon the ratio of image centers falling inside the aperture to those falling outside. For model 2 which had the largest error in calculated efficiency, this ratio was much larger than for model 1 or an electroformed nickel concentrator reported in reference 5.

Geometric efficiencies calculated from ray-trace data can provide useful information and reduce the calorimetric testing required but even the most reliable method used in this investigation, the random error method, had errors in efficiency of up to 0.07.

### Vibration

Vibration tests were performed on model 1 to determine its resonant frequencies and the ability of the structure to withstand simulated launch loads.

The resonant frequencies of the concentrator shell, while simply suspended, were determined to be 18, 25, and 39 Hz. The nodal patterns in the shell are shown in figure 15. The first two nodal patterns (18 and 25 Hz) are similar to those shown in reference 12 for a concentrator of comparable size and shell geometry. However, the third nodal pattern for the reference 12 model had three nodal lines similar to a superposition of the first and second modes. The third nodal pattern (fig. 15, 39 Hz) for the present model rotated about the concentrator axis with change in exciter position but the basic pattern remained unchanged. A resonance in the rim support ring was noted at 70 Hz but no shell nodes were detected.

Following the simple suspension test the concentrator was placed on the electrodynamic vibration exciter and tested at a 1g input level (run 1, table 1(b)) to determine the resonant frequencies under the stiffer mounting configuration. The axial shell deflection at the concentrator vertex and the radial response parallel to the input excitation axis (accelerometer 4) and at an angle of  $\pi/3$  rad with the input excitation axis (accelerometer 2) are shown in figure 16. The axial shell deflection (fig. 16(a)) at the shell center indicated resonances in the shell near 29 and 37 Hz, but it was not determined to which vibratory modes these correspond. The shell excursions near 58 and 80 Hz appeared to be the result of rim support ring resonance, as indicated by the high vibration levels recorded by the accelerometers which were mounted near the ring. The magnitude of the response at 80 Hz could not be determined as the response became so large that adjoining oscillograph traces overlapped and became illegible. This resonance probably corresponds to the rim support ring resonance noted at 70 Hz during the simple suspension test; however, the frequency was higher because of the stiffer mounting provided by the standoff mounts. The resonant conditions above 100 Hz, as indicated by the accelerometer traces, were not specifically identified as being ring or shell resonances.

Following the 1g test to determine the resonant frequencies, the launch simulation test was begun. Because of difficulty with the test equipment, run 2 was at 2.1g instead of the prescribed 3.0g (table 1) and run 3 was at 3.5g instead of the prescribed 4.9g. Following run 3 some slight separation of the welds at the bottom of the rim support ring was noted and an additional 1g sweep was made (run 4) to determine if the resonant frequencies had changed. Subsequent analysis of the data from run 4 indicated that the resonant frequencies were lower than for run 1 but a visual inspection of the concentrator indicated that the shell had not been adversely affected, therefore the test program was continued. During run 6 (4.9g test level) at an excitation of about 45 Hz, the welds holding one of the mounting brackets failed, allowing the bracket to separate from the rim support ring. No additional launch simulation tests were run; however, the bracket was repaired and runs 7 to 11 were made to test the integrity of the shell. During these runs the support welds at the bottom of the rim support ring continued to separate. Separations about 30 cm long and similar to that shown in figure 17 had occurred near each support bracket by the end of run 11; consequently, the tests were terminated.

Following the vibration test, the concentrator was again placed on the solar tracker for calorimetric tests to determine if the shell had been damaged. The calorimeter was moved about the focal region to determine the maximum efficiency at each of several aperture sizes. Variation in calorimetric efficiency with aperture size before and after the vibration test is compared in figure 18(a). The 0.05 loss at the largest aperture size indicates a loss in specular reflectance that occurred over the duration of the investigations. Therefore, each set of data was divided by its specular reflectance to obtain geometric efficiency. The variation in geometric efficiency with aperture size before

and after vibration tests is presented in figure 18(b). At aperture radius ratios of 2 to 3 suitable for thermionic converters the decrease in geometric efficiency after vibration is only about 0.04. Since the accuracy of data is  $\pm 0.02$ , the loss in concentrator efficiency due to vibration appears to be small.

### CONCLUDING REMARKS

Three stretch-formed aluminum solar concentrators representing three phases of a stretch-forming development program have been evaluated for possible use with thermionic converters. Model 3, which represented the third phase, had the highest geometrical accuracy and specular reflectance of any model tested. The calorimetric efficiency of this model was 0.85 at an aperture radius of 2.5 solar images (considered suitable for thermionic applications), which is only about 0.05 lower than the efficiency the model would have had with perfect geometry. It is therefore considered suitable for use with thermionic converters. The increase in efficiency of this model over models 1 and 2 may be attributed to improvements in design and fabrication developed during the program. Models 1 and 2 were optically tested and compared with published data for model 3. These tests permitted the location and magnitude of surface slope errors to be determined and improvements in the fabrication techniques to be evaluated. Comparison of the slope errors on the three models confirmed the results of the calorimetric tests which indicated an improvement in geometry with each phase of development. The surface slope errors were largest near the sector seams but this region of large error extended only to the edge of the overlap strip. The surface slope errors were used to calculate geometric efficiencies. The calculated geometric efficiency can provide useful information and reduce the calorimetric testing required to evaluate concentrator performance. Vibration tests were performed on model 1. Failure of the support structure to withstand flight qualification tests did not impair the geometrical accuracy of the shell.

Langley Research Center,  
National Aeronautics and Space Administration,  
Langley Station, Hampton, Va., June 24, 1968,  
120-33-06-08-23.

## REFERENCES

1. Anon.: Electrical Power Generation Systems for Space Applications. NASA SP-79, 1965.
2. Wilson, Volney C.; and Hamilton, Robert C.: Thermionic Converters for Space Power. Astronaut. Aerosp. Eng., vol. 1, no. 4, May 1963, pp. 62-67.
3. Houck, O. K.; and Heath, A. R., Jr.: Characteristics of Solar Concentrators as Applied to Space Power Systems. Paper 867C, Soc. Automot. Eng., Apr. 1964.
4. Willis, Conrad M.: Calorimetric Evaluation of a 60-Inch (152-Centimeter) Electroformed Nickel Solar Concentrator. NASA TN D-3012, 1965.
5. Willis, Conrad M.; and Houck, O. Karl: Geometric Efficiency of an Electroformed Nickel Solar Concentrator. NASA TN D-4072, 1967.
6. Castle, Charles H.: Final Report - Fabrication of a 60 Inch Diameter Stretch Formed Aluminum Solar Concentrator. ER-5048, Thompson Ramo Wooldridge Inc., Sept. 14, 1962.
7. Thompson Ramo Wooldridge, Inc.: 60-Inch Stretch-Formed Aluminum Solar Concentrator. NASA CR-47, 1964.
8. Anon.: Stretch-Formed Aluminum Solar Concentrator. TRW ER-6819 (NASA CR-66069), TRW Equip. Lab., TRW Inc., Apr. 1966.
9. Comm. on Metric Pract.: ASTM Metric Practice Guide. NBS Handbook 102, U.S. Dep. Com., Mar. 10, 1967.
10. Herr, Robert W.; and Carden, Huey D.: Support Systems and Excitation Techniques for Dynamic Models of Space Vehicle Structures. Proceedings of Symposium on Aeroelastic & Dynamic Modeling Technology, RTD-TDR-63-4197, Pt. I, U.S. Air Force, Mar. 1964, pp. 249-277.
11. Menetrey, W. R.: Solar Energy Thermionic Conversion System. Rep. 1850-Final (Contract No. JPL-950109), Electro-Opt. Syst., Inc., Jan. 15, 1962.
12. Leppert, E. L., Jr.: Vibration Tests of Prototype Five Foot Solar Concentrator. D2-20877, Boeing Co., [1962].
13. Schrenk, G. L.; and Gritton, D. G.: Analysis of Solar Reflectors - Mathematical Theory and Methodology for Simulation of Real Reflectors. EDR 3693 (Contract AF04(695)-335), Allison Div., Gen. Motors Corp., Dec. 16, 1963. (Available from DDC as AD 602 870.)

**TABLE 1.- LAUNCH VIBRATION SIMULATION TEST  
SPECIFICATIONS AND CONDITIONS**

(a) Vibration test specifications\*

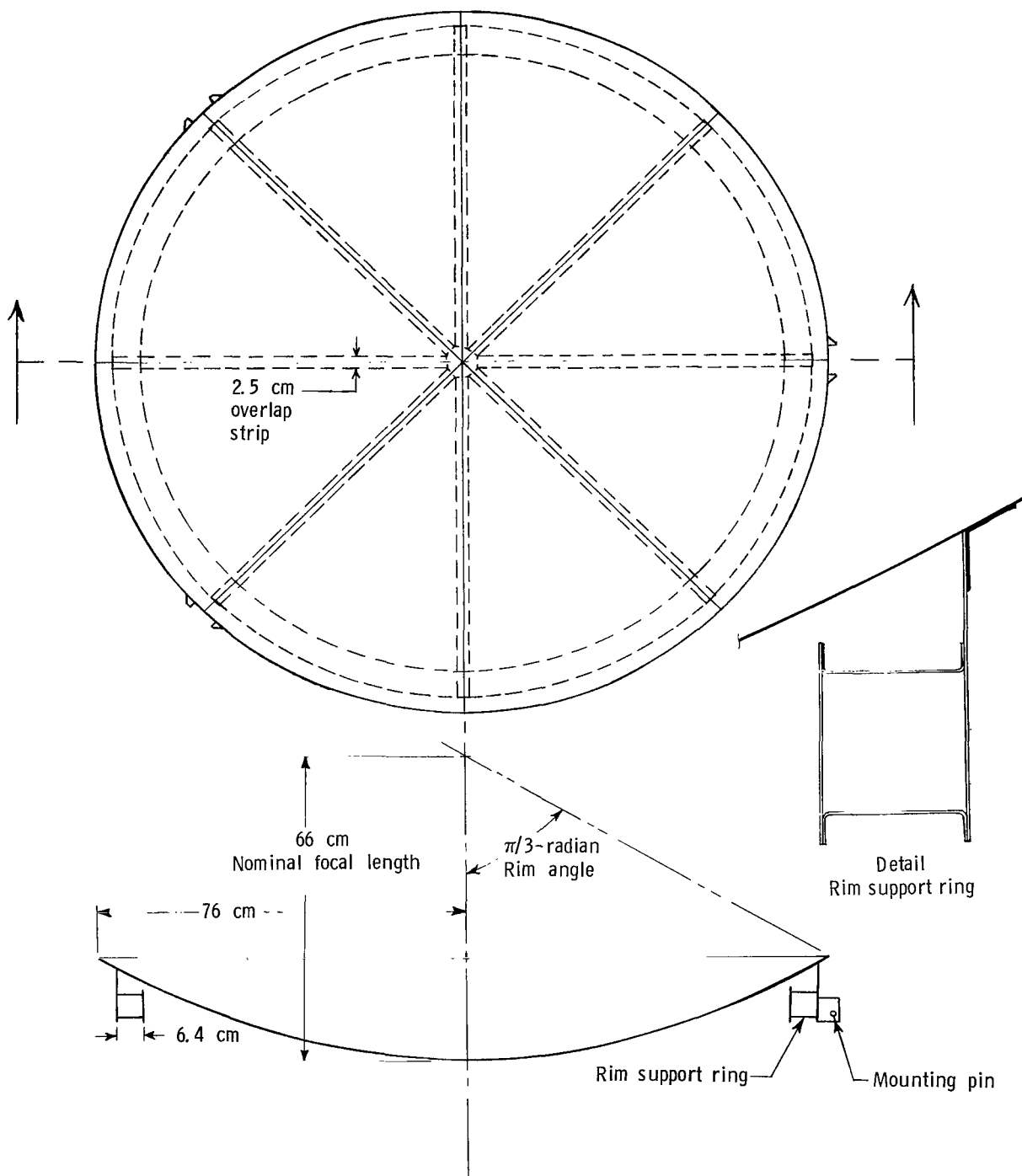
Frequency range, Hz	Test level g units	Type of excitation
15 to 40	±3.0	Sine wave
40 to 1500	±4.9	Sine wave
15 to 1500	1.5 (rms)	White noise

\*Specifications indicated test loads should be applied along three orthogonal axes at a sweep rate of 2 octaves per minute. Failure of the concentrator mounting bracket during run 6 prevented completion of the test program.

(b) Vibration test conditions

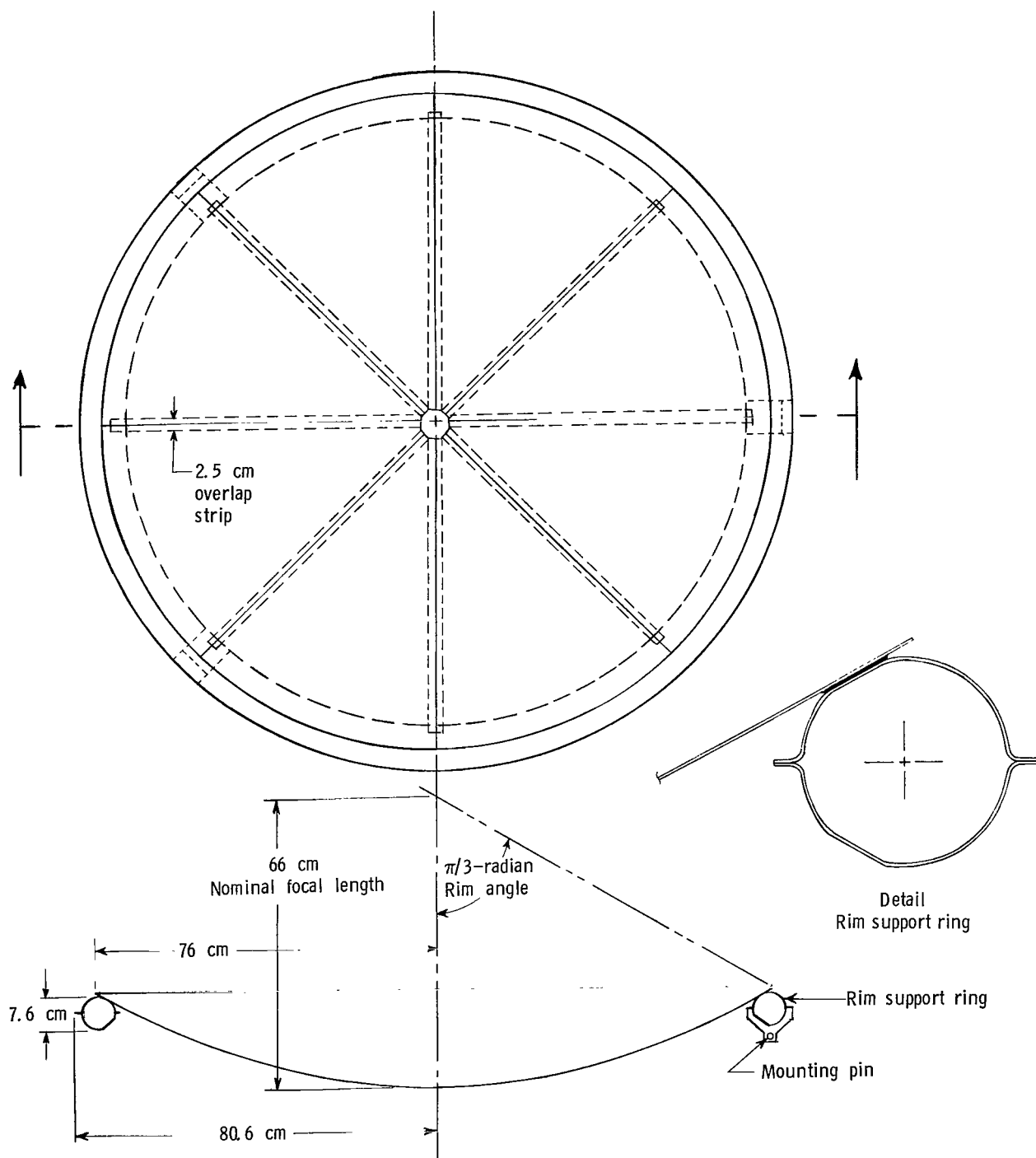
Run	Test level g units	Type of excitation	Frequency range, Hz	Excitation axis (fig. 7)	Plane of accelerometer axis
1	±1	Sine wave	15 to 1500	1	Radial
2	±2.1	Sine wave	15 to 40	1	Radial
3	±3.5	Sine wave	40 to 1500	1	Radial
4	±1	Sine wave	15 to 1500	1	Radial
5	±3	Sine wave	15 to 40	1	Radial
6	±4.9	Sine wave	40 to 45	1	Radial
7	0.0015 g <sup>2</sup> /Hz	White noise	15 to 1500	1	Radial
8	±1	Sine wave	15 to 1500	1	Concentrator axis
9	±1	Sine wave	15 to 1500	1	Concentrator axis
10	±1	Sine wave	15 to 1500	2	Concentrator axis
11	±1	Sine wave	15 to 1500	2	Radial





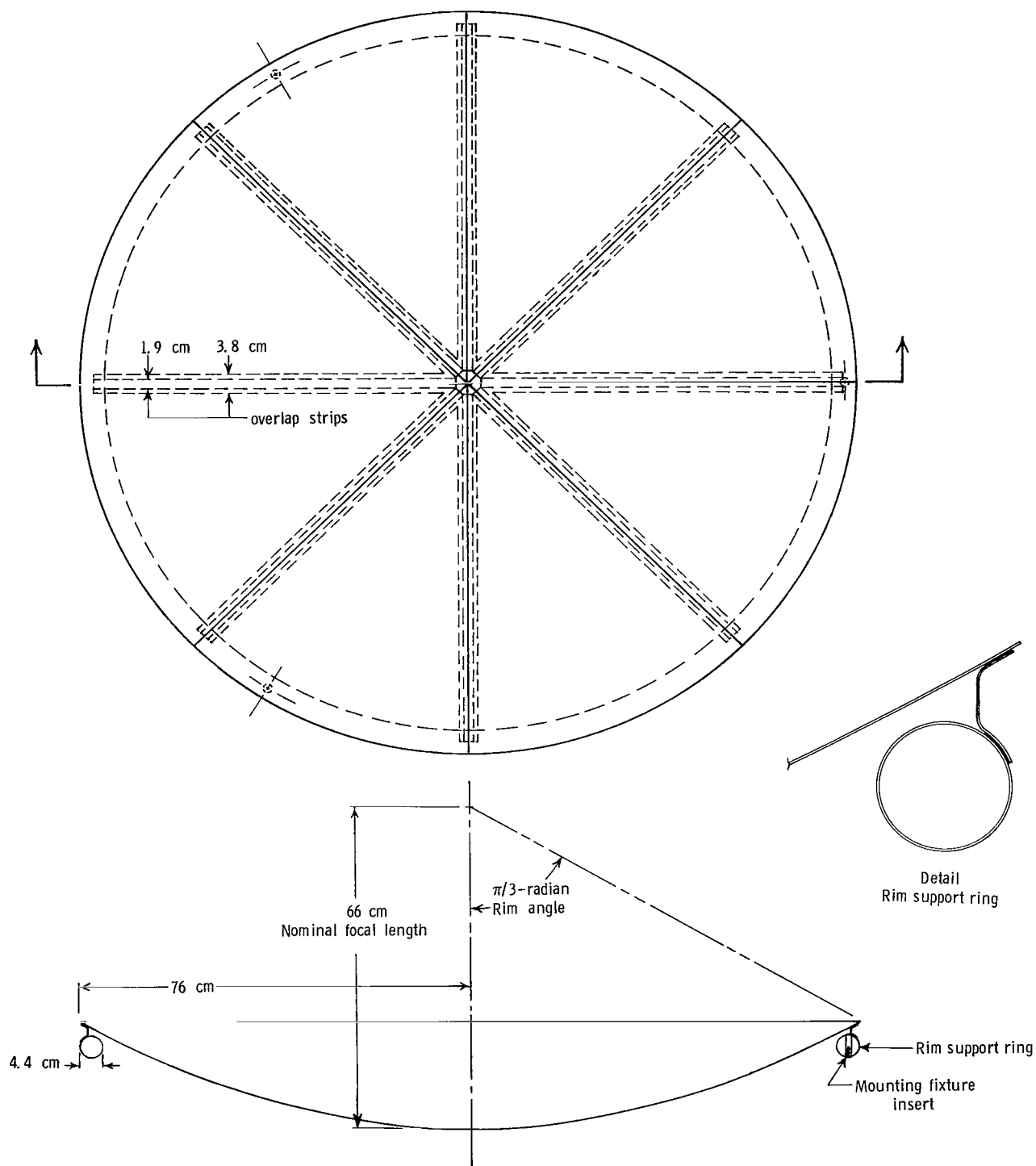
(a) Model 1.

Figure 1.- Solar concentrator models.



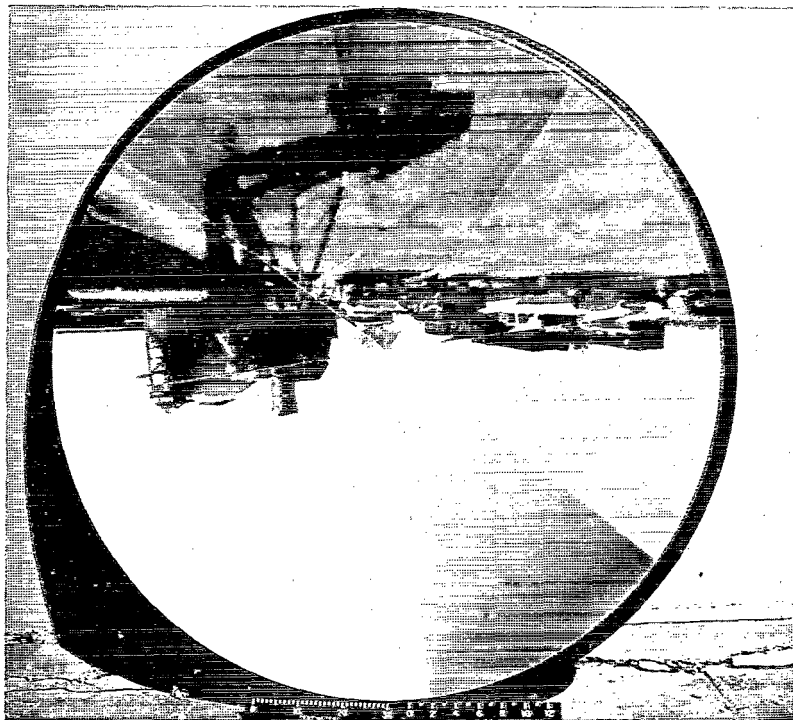
(b) Model 2.

Figure 1.- Continued.



(c) Model 3.

Figure 1.- Concluded.



L-65-2992

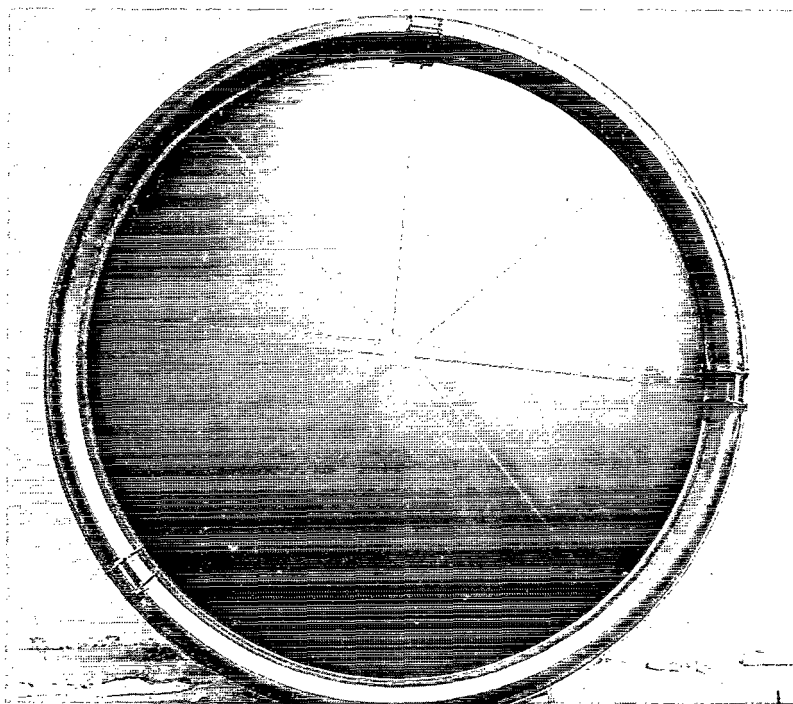


Figure 2.- Front- and rear-view photographs of solar concentrator. Model 2. L-65-2993

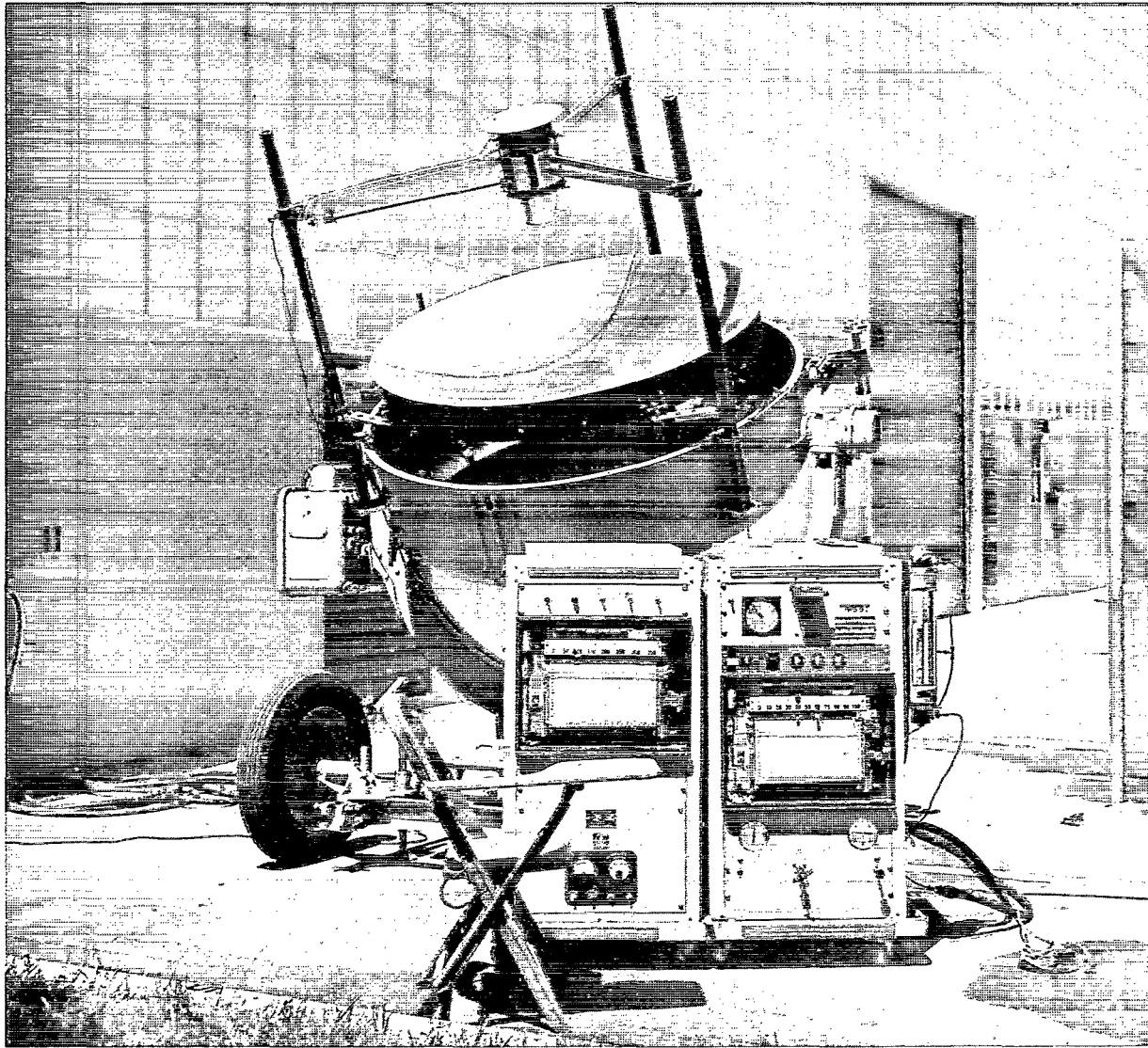


Figure 3.- Concentrator mounted on solar tracker for calorimetric efficiency tests.

L-64-5455

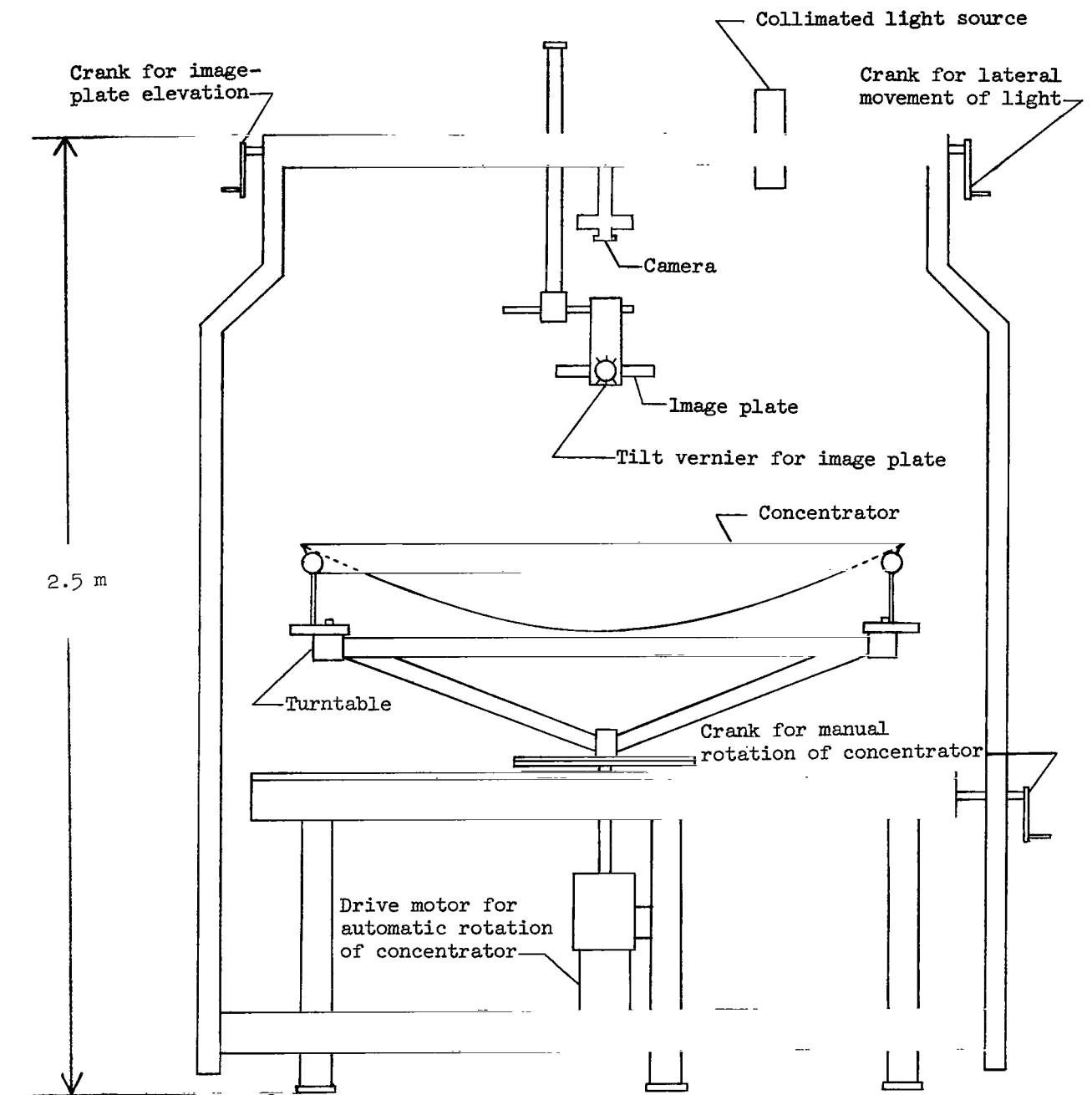


Figure 4.- Sketch of optical test fixture.

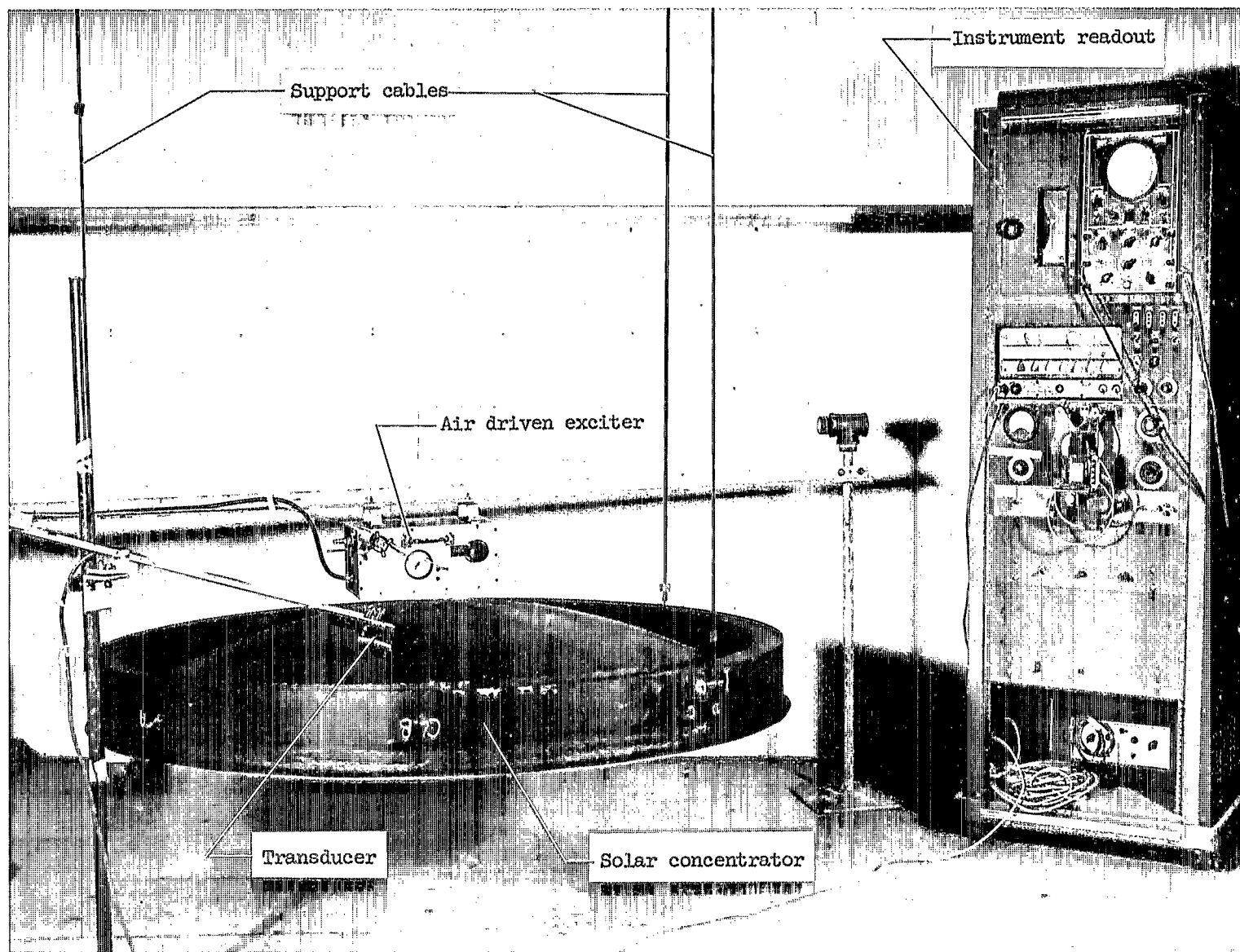


Figure 5.- Test setup to determine natural frequencies.

L-64-1502.1

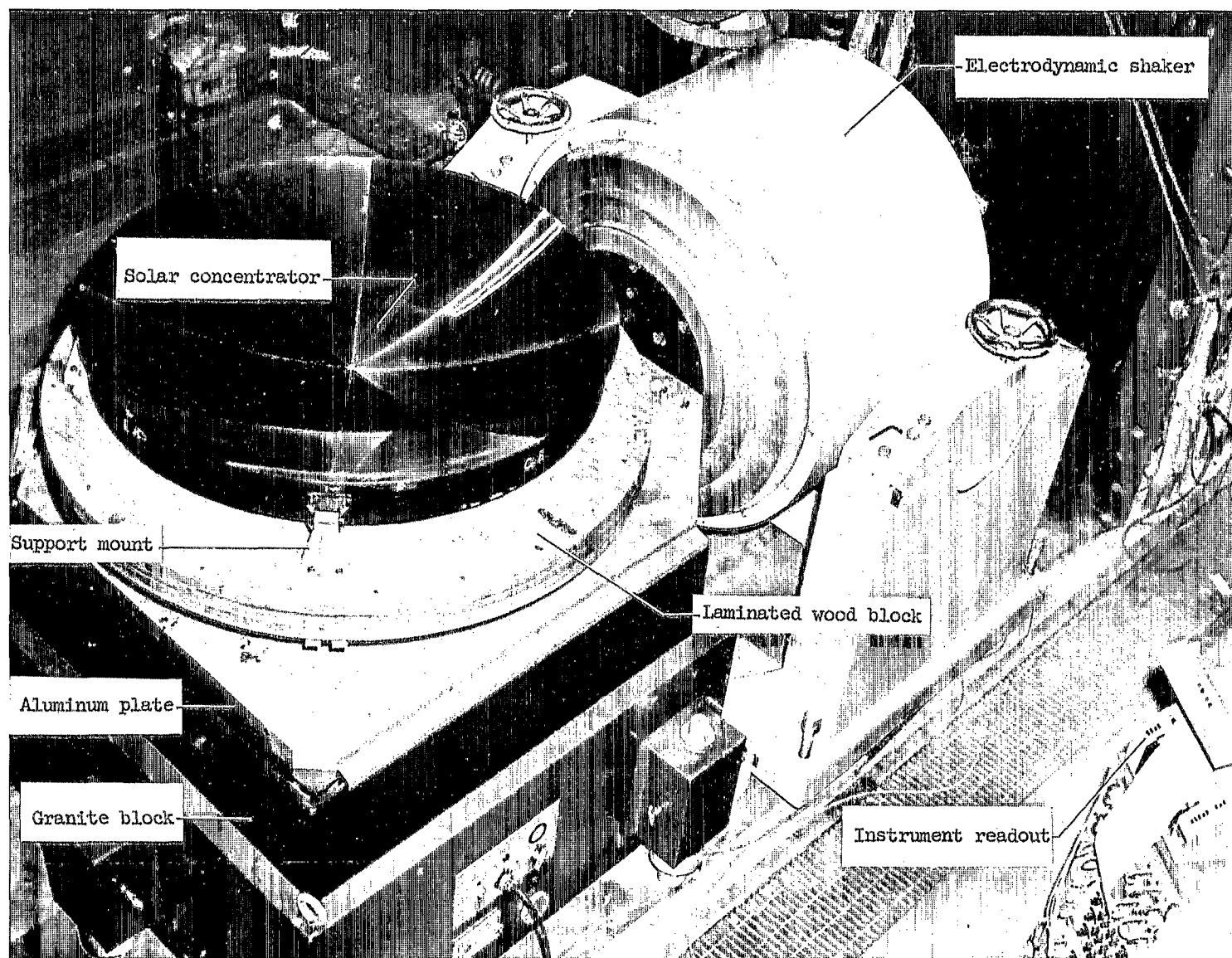


Figure 6.- Test setup for launch vibration environment.

L-64-2088.1

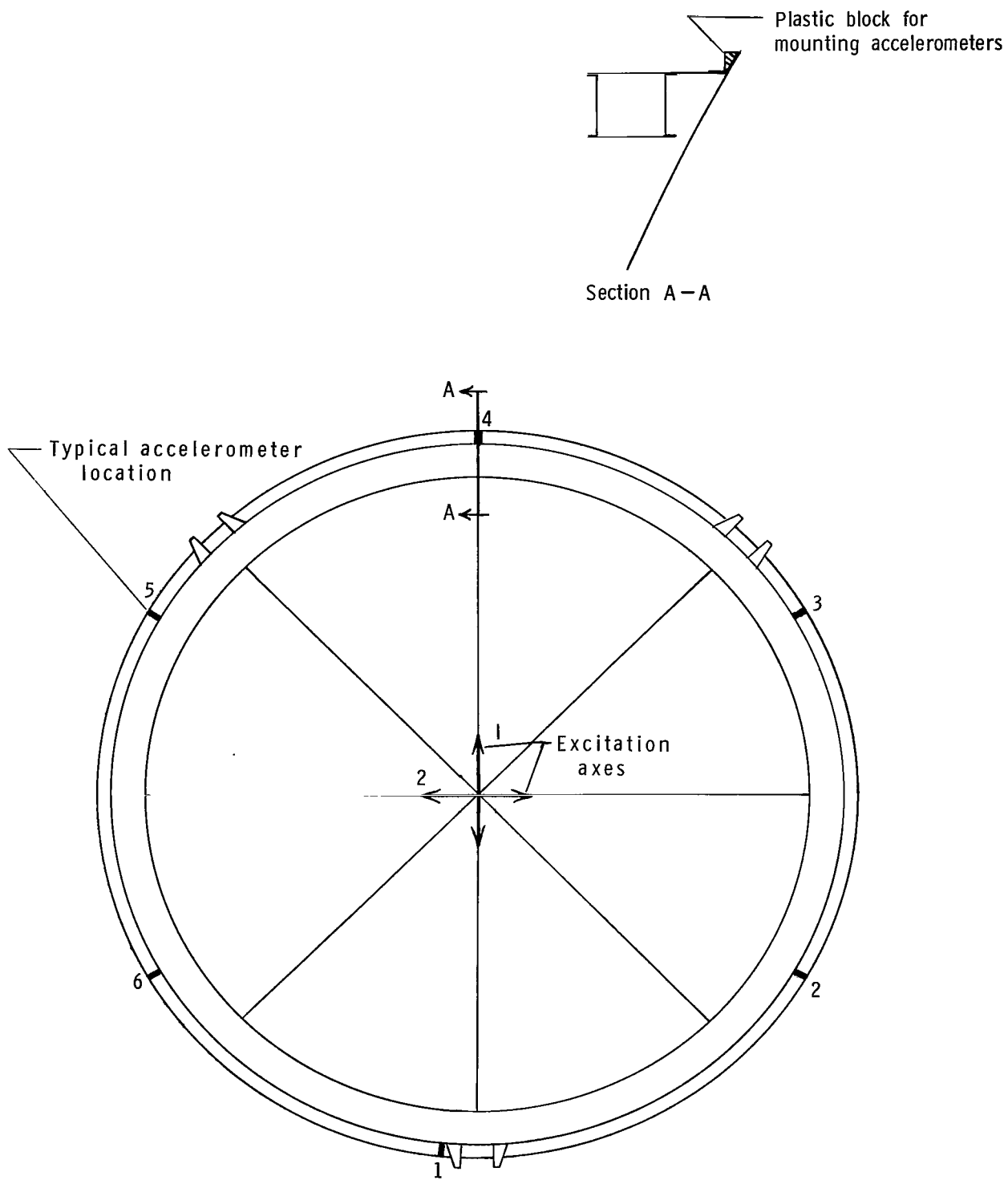
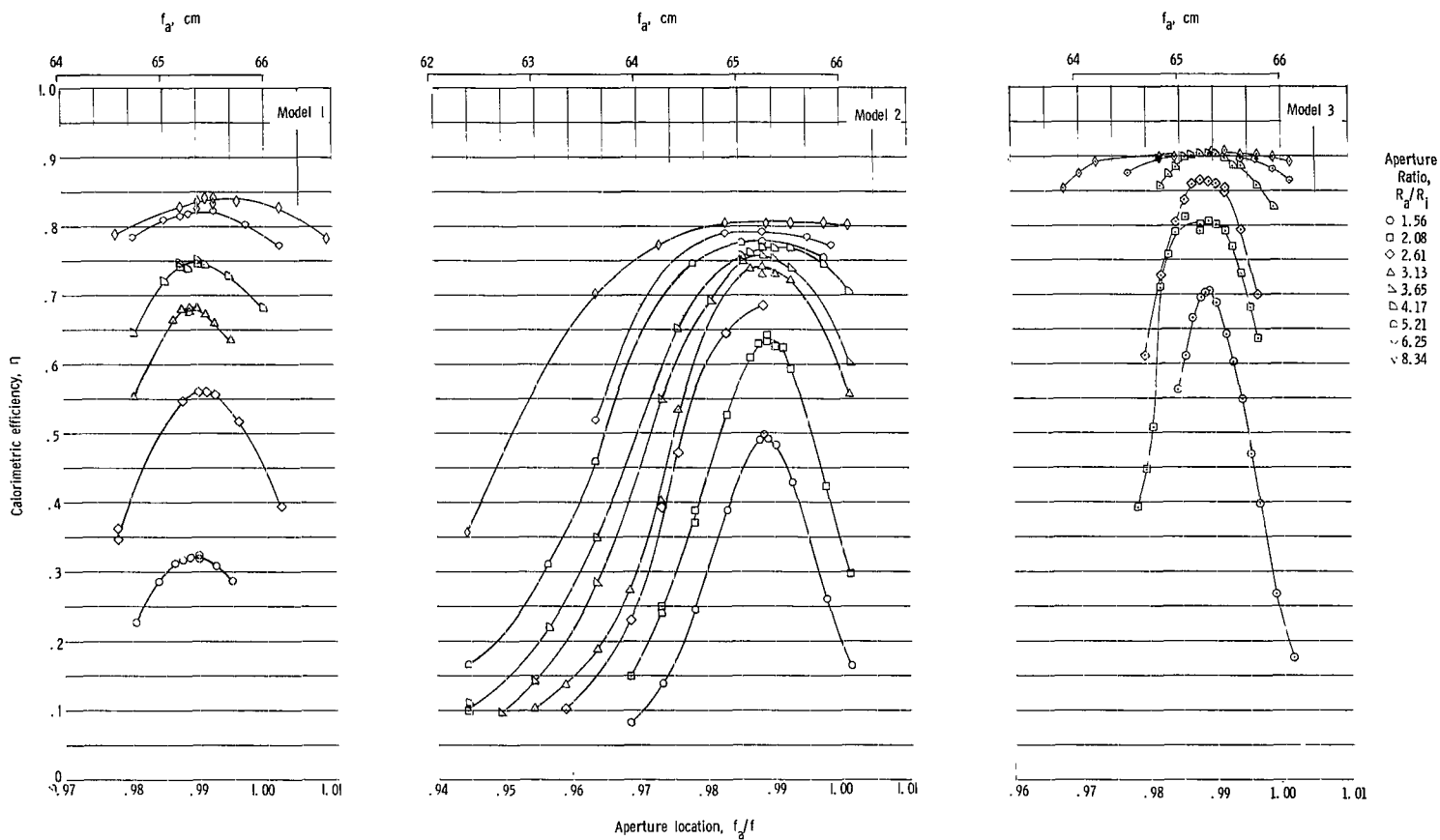
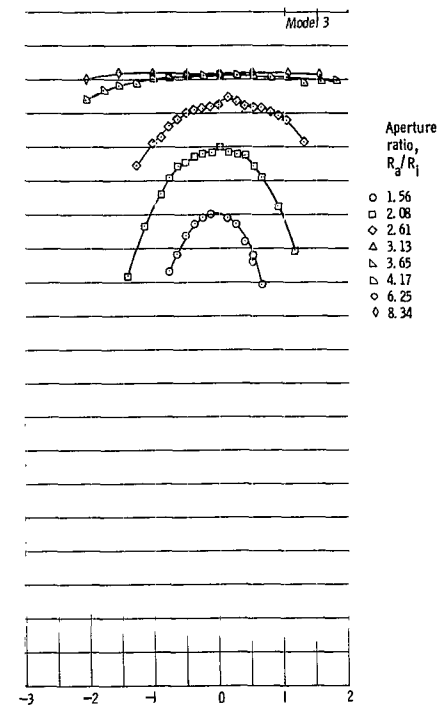
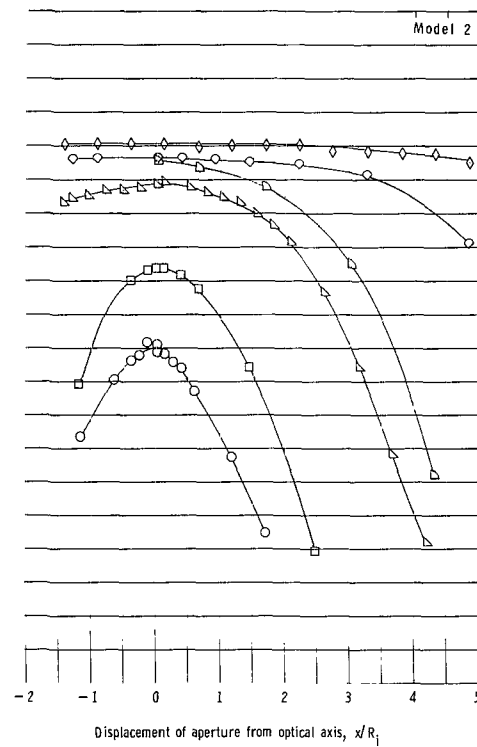
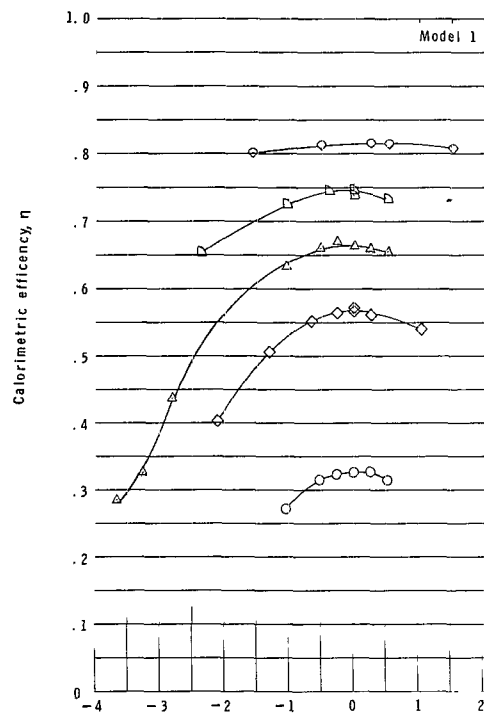


Figure 7.- Sketch showing excitation axes and accelerometer locations.



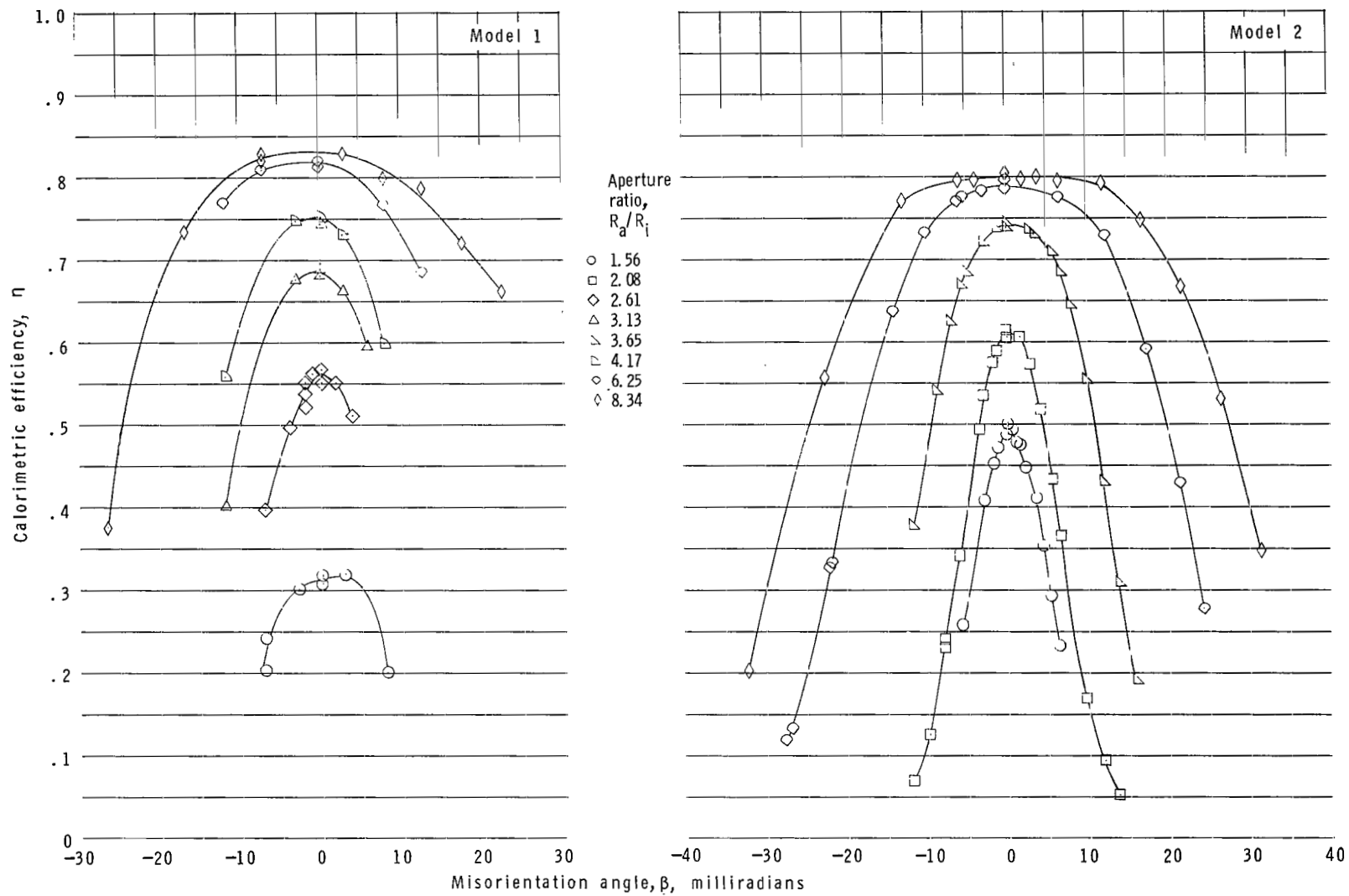
(a) Variation in efficiency with axial location of calorimeter.

Figure 8.- Calorimetric efficiency of all models.



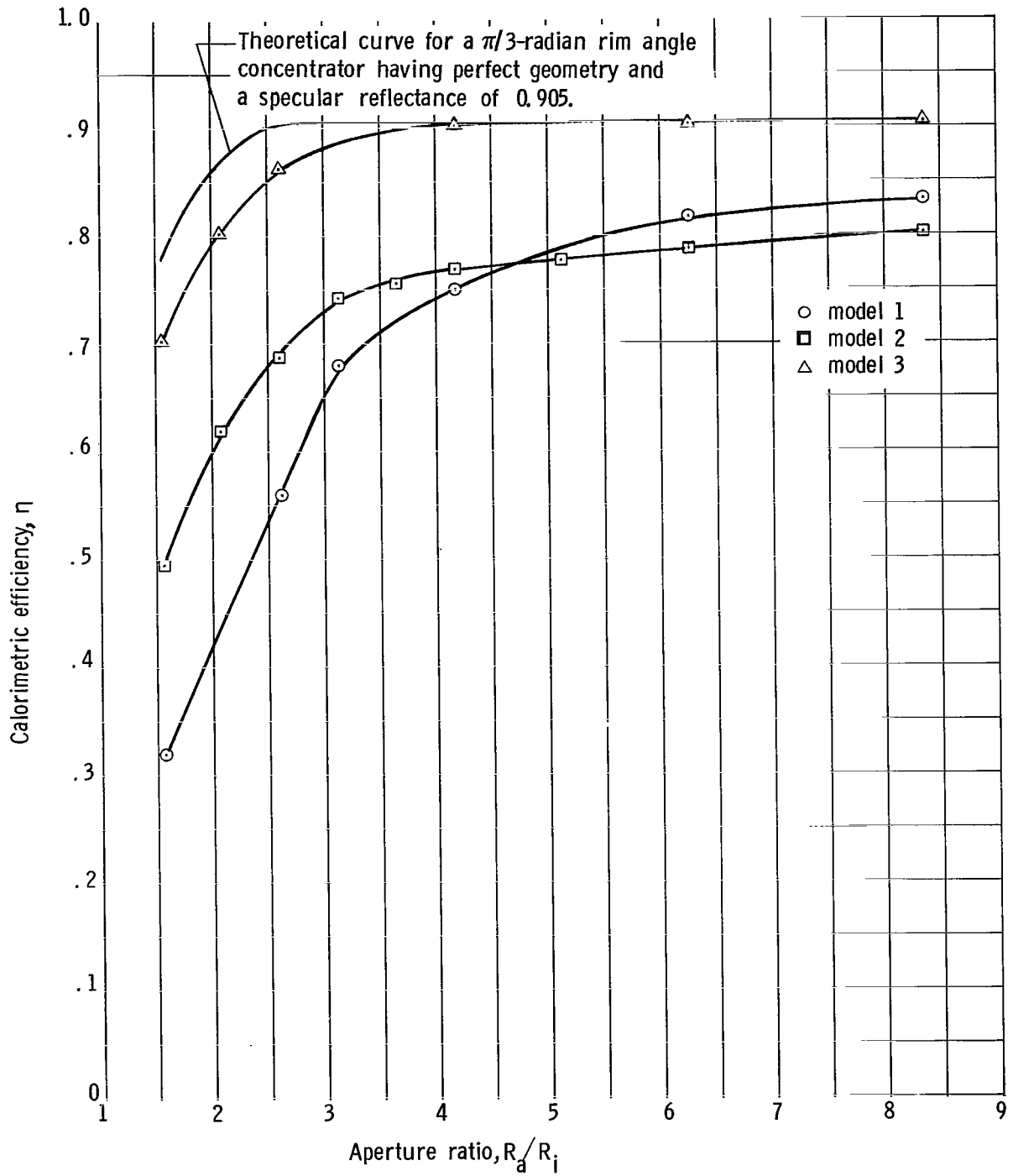
(b) Variation in efficiency with lateral location of calorimeter.

Figure 8.- Continued.



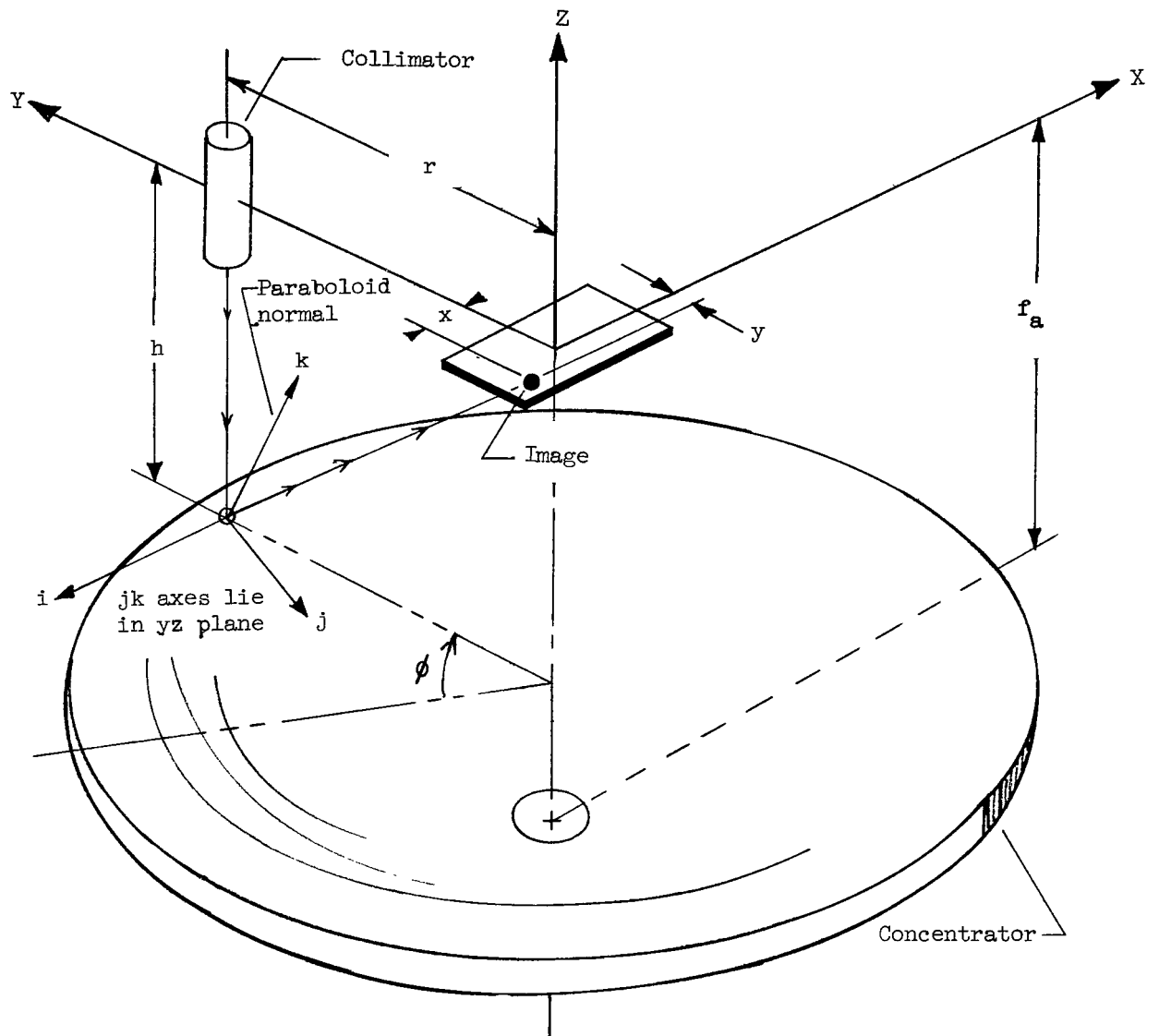
(c) Variation in efficiency with misorientation of the concentrator axis with the solar rays.

Figure 8.- Continued.



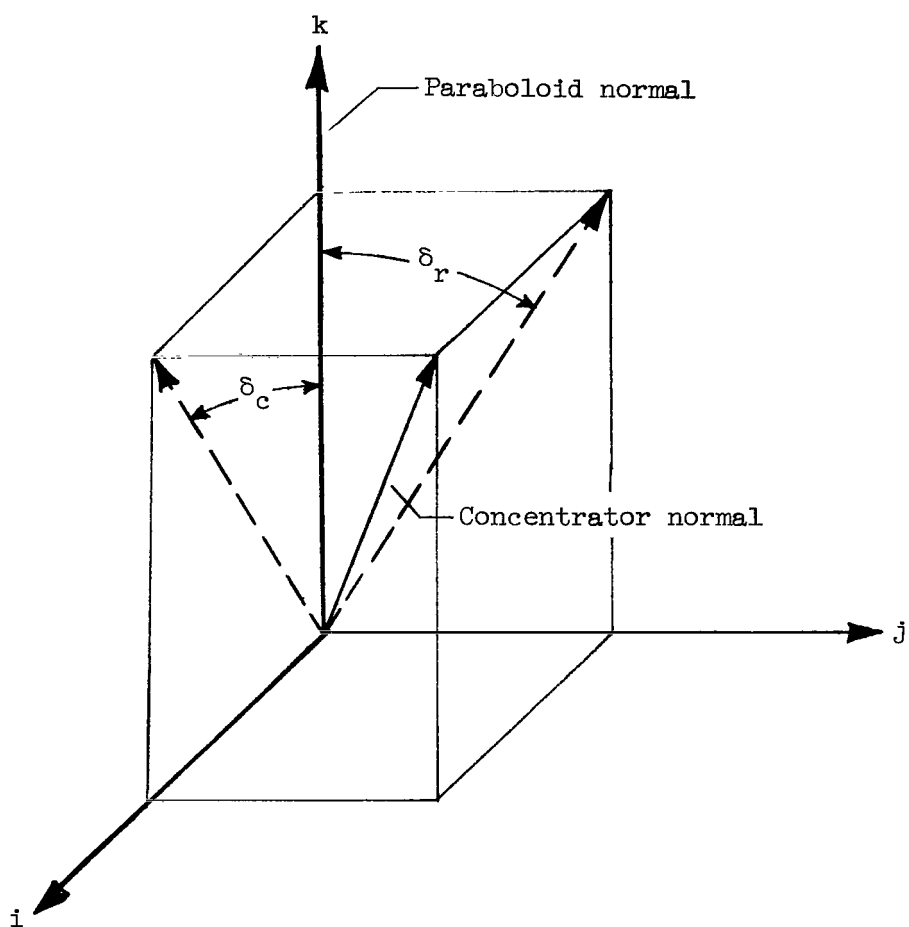
(d) Variation in efficiency with aperture size.

Figure 8.- Concluded.



(a) Coordinate systems.

Figure 9.- Sketches defining coordinate systems and slope error angles.



$$\delta_r = \tan^{-1} \frac{r}{2f_a} - \tan^{-1} \frac{r-y}{h + \sqrt{x^2 + h^2 + (r-y)^2}}$$

$$\text{where } h = f_a - \frac{r^2}{4f_a}$$

$$\delta_c = \tan^{-1} \left[ \frac{-ax}{\cos \delta_r (r-y) (\alpha^2 + h^2)^{1/2}} \right]$$

$$\text{where } a = \frac{h(r-y)}{h + \sqrt{x^2 + h^2 + (r-y)^2}}$$

(b) Slope error angles of the reflective surface.

Figure 9.- Concluded.

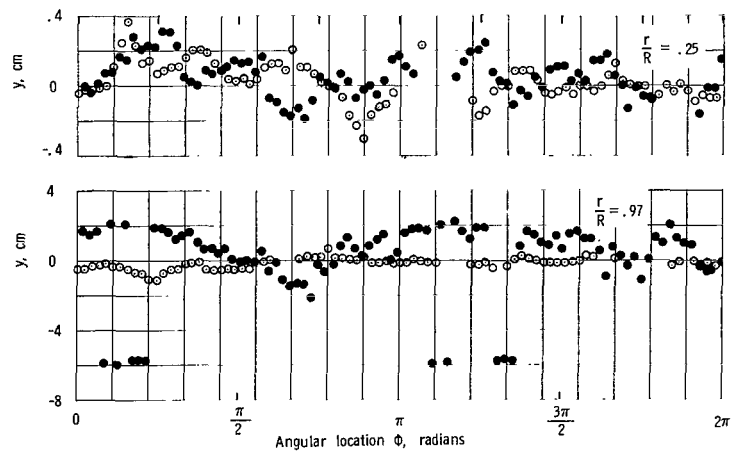
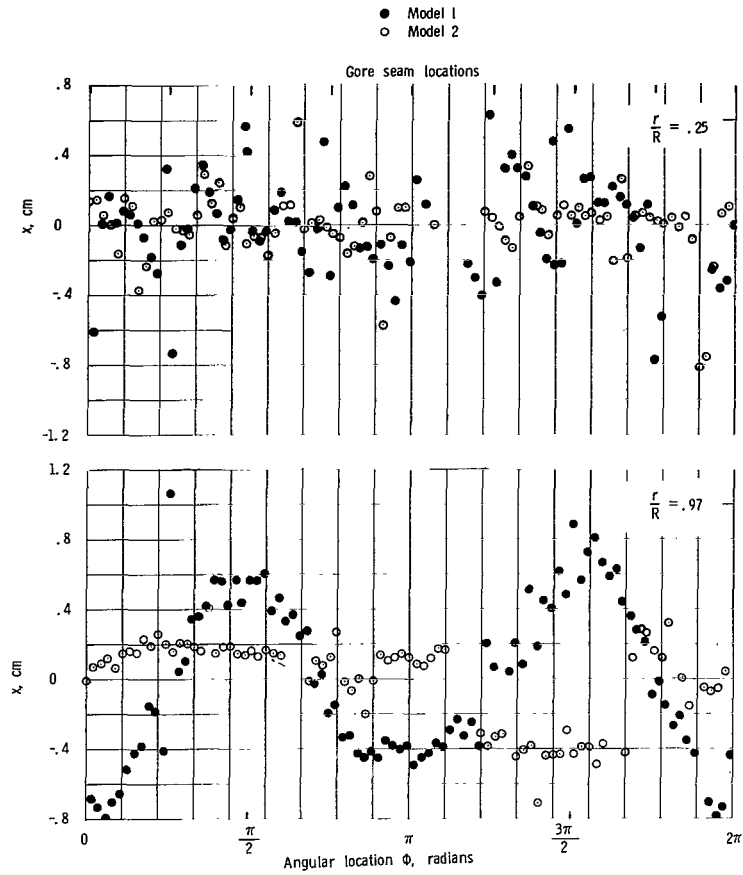


Figure 10.- Components of image displacement for two radial locations of the concentrator.

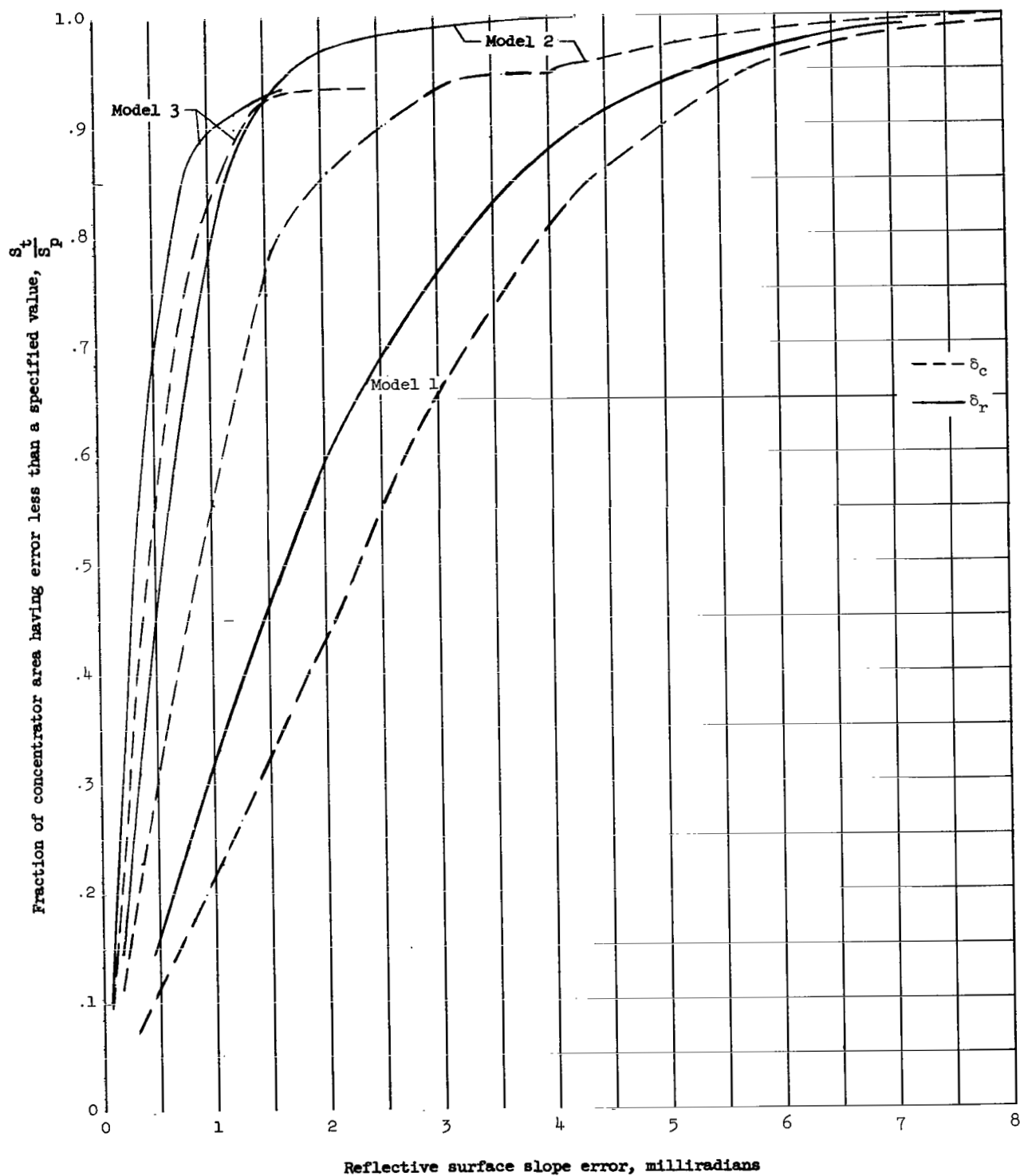
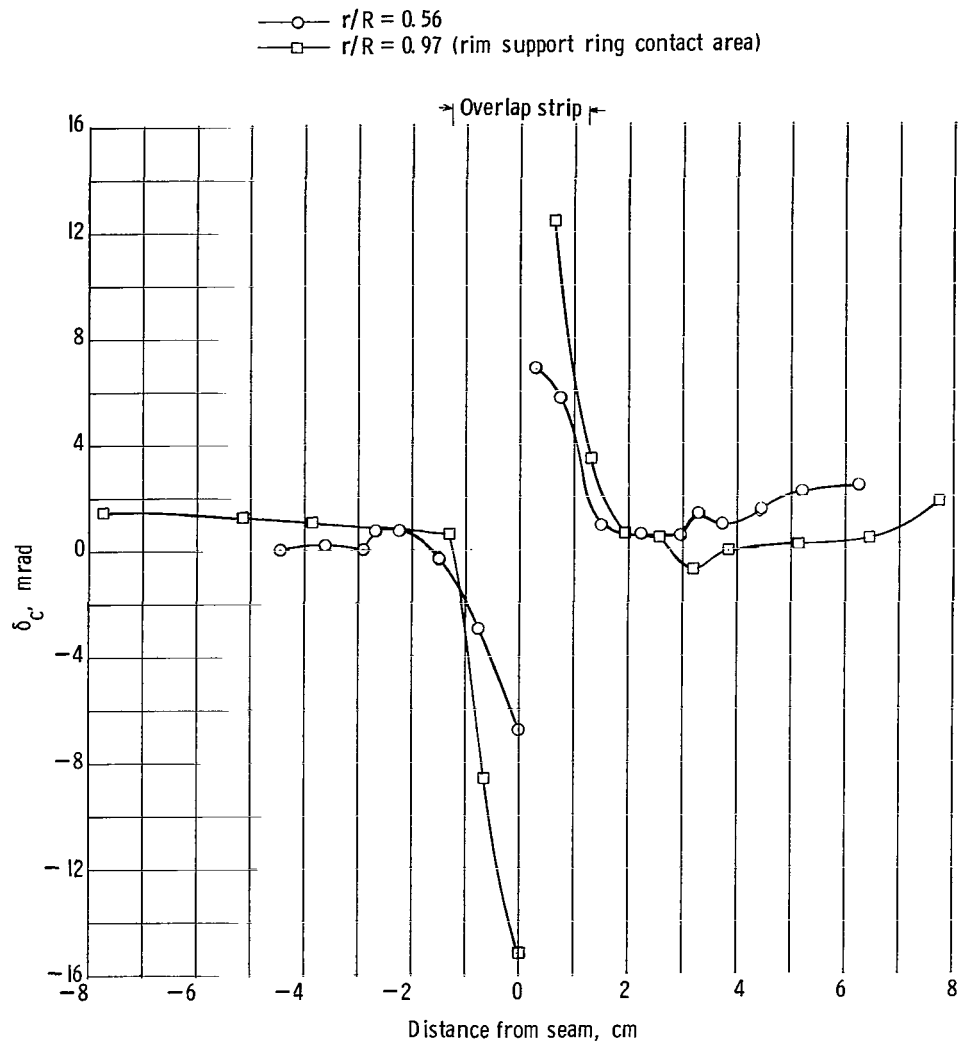
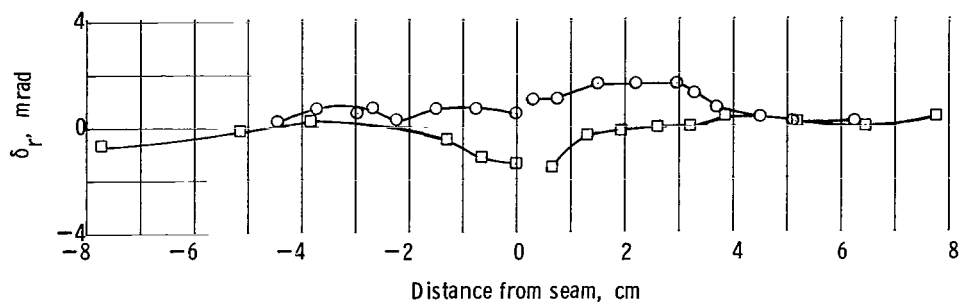


Figure 11.- Cumulative distribution of surface slope errors.

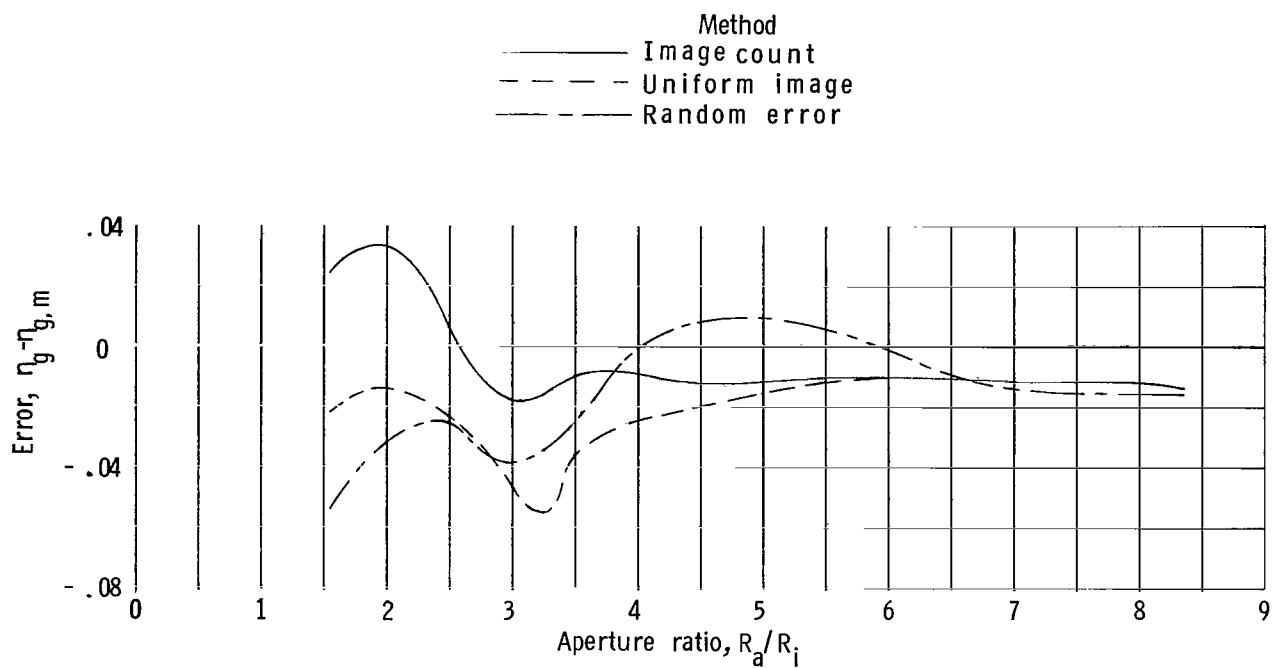


(a) Circumferential error.

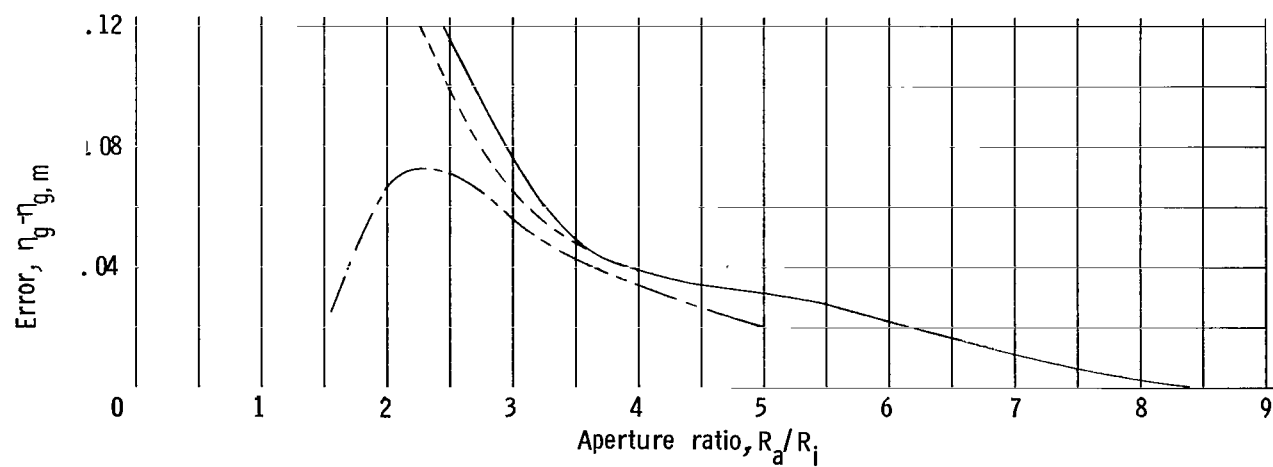


(b) Radial error.

Figure 12.- Variation in surface slope error across sector seam. Model 2.

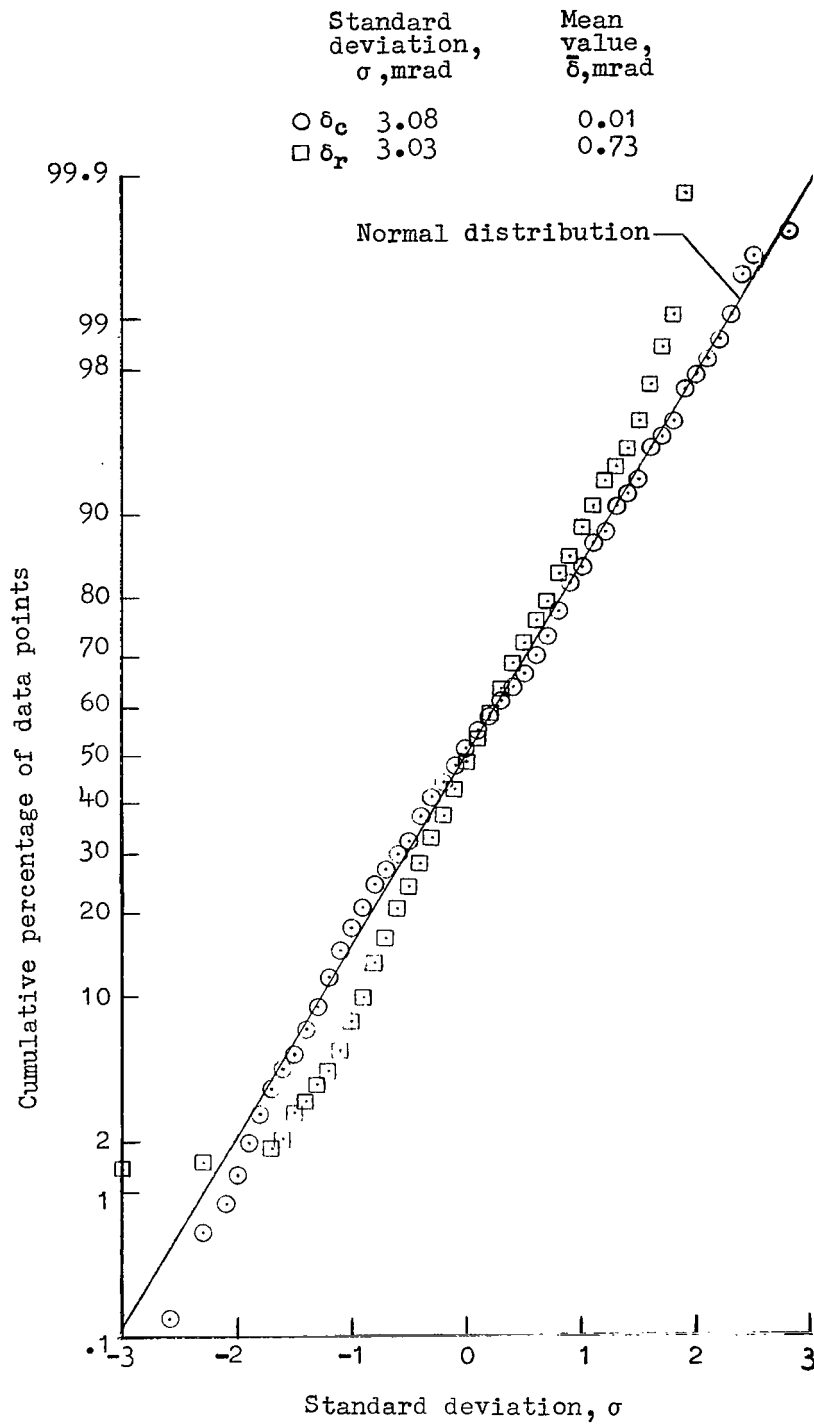


(a) Model 1.



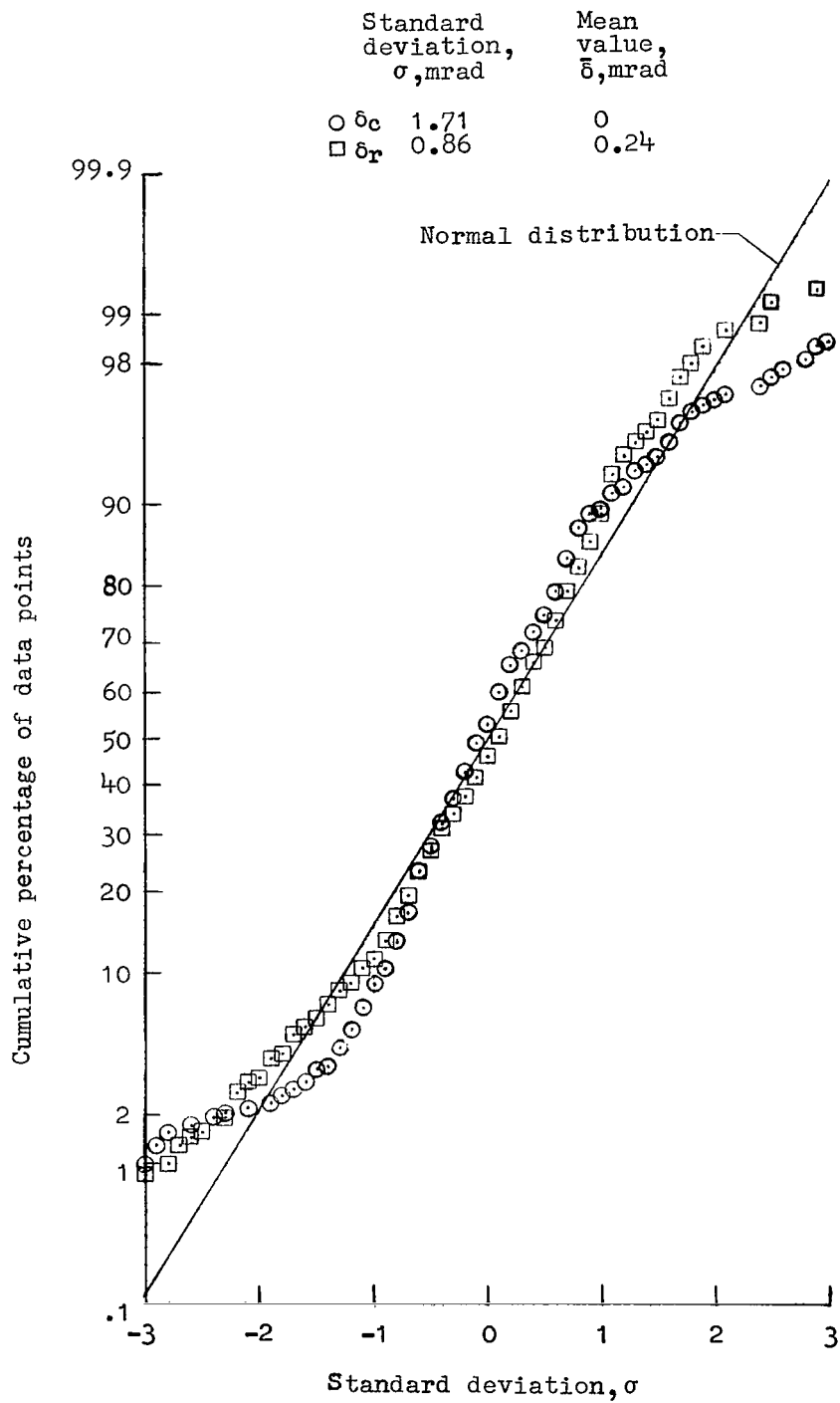
(b) Model 2.

Figure 13.- Error in geometrical efficiency for various methods of calculation.



(a) Model 1.

Figure 14.- Comparison of concentrator slope errors to a normal distribution.



(b) Model 2.

Figure 14.- Concluded.

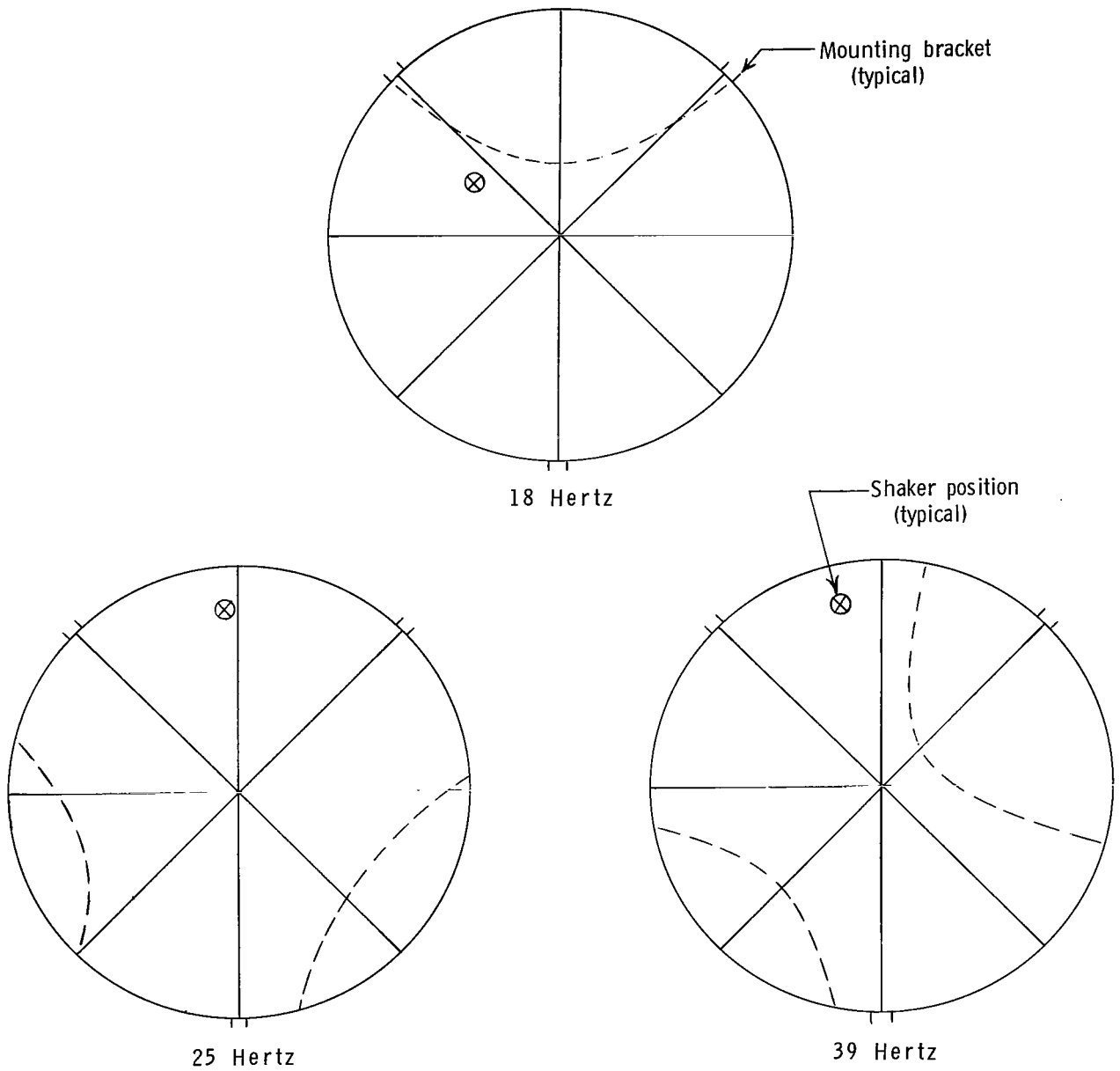
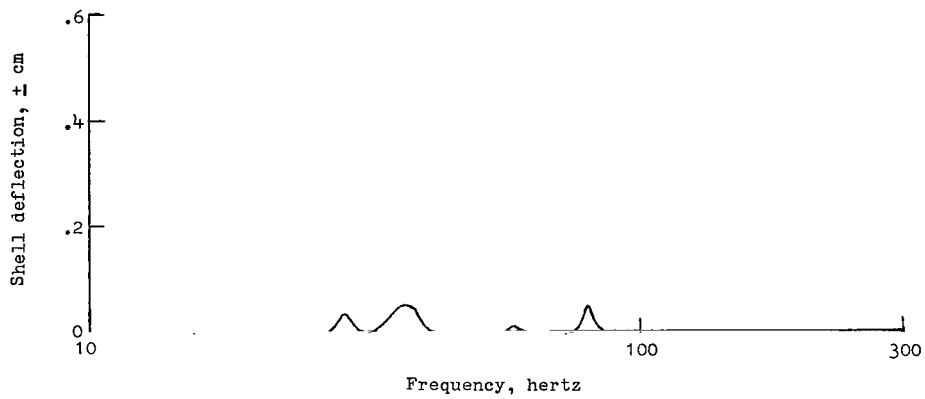
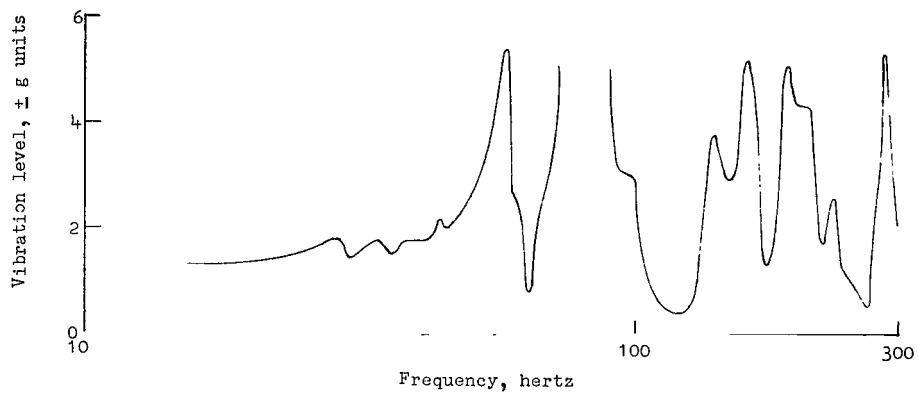


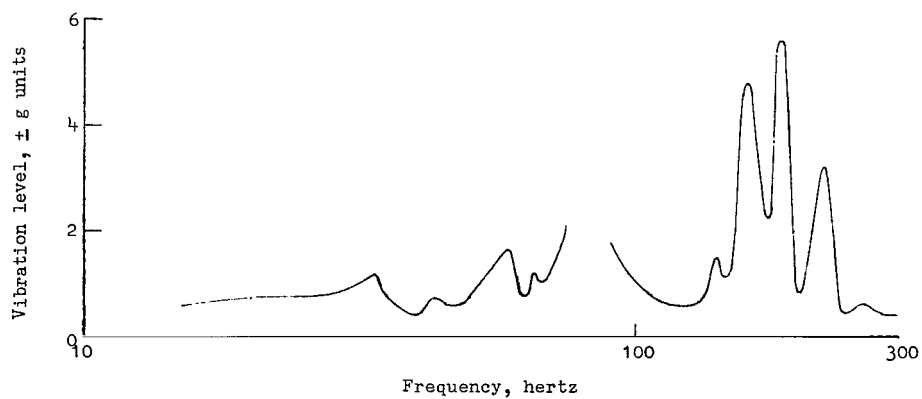
Figure 15.- Nodal patterns in concentrator shell. Model 1.



(a) Axial deflection of shell vertex.



(b) Concentrator response parallel to excitation axis. Accelerometer 4.



(c) Concentrator response at an angle of  $\pi/3$  rad with the input excitation axis. Accelerometer 2.

Figure 16.- Response of concentrator to a 1g input along a transverse axis (axis 1).

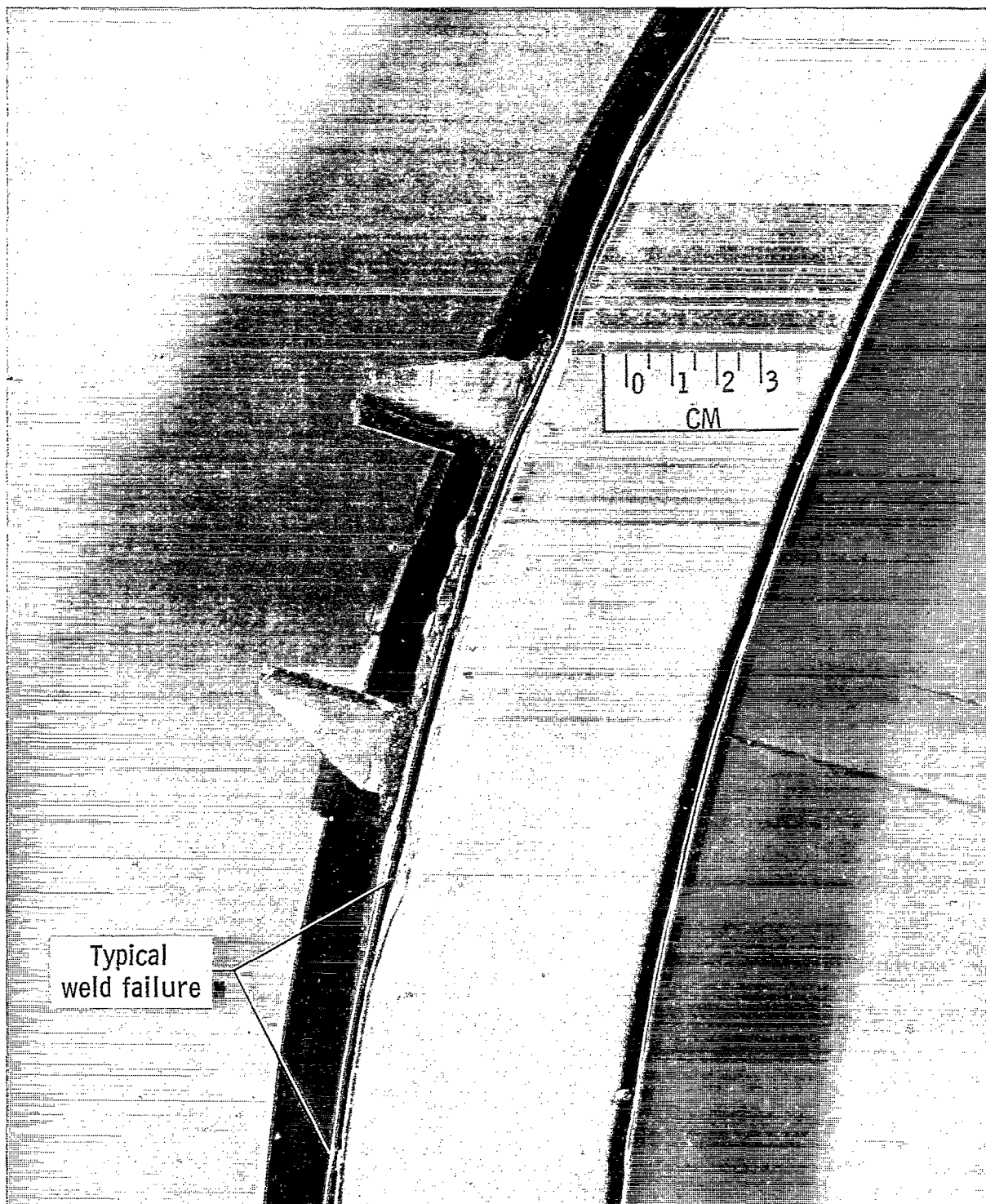
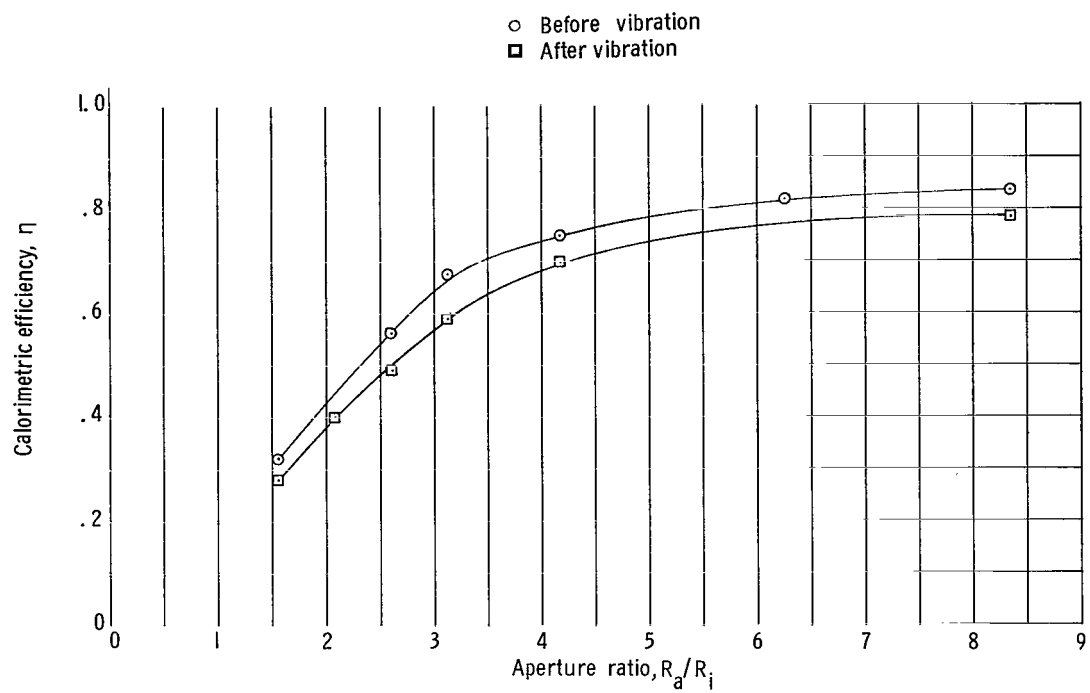
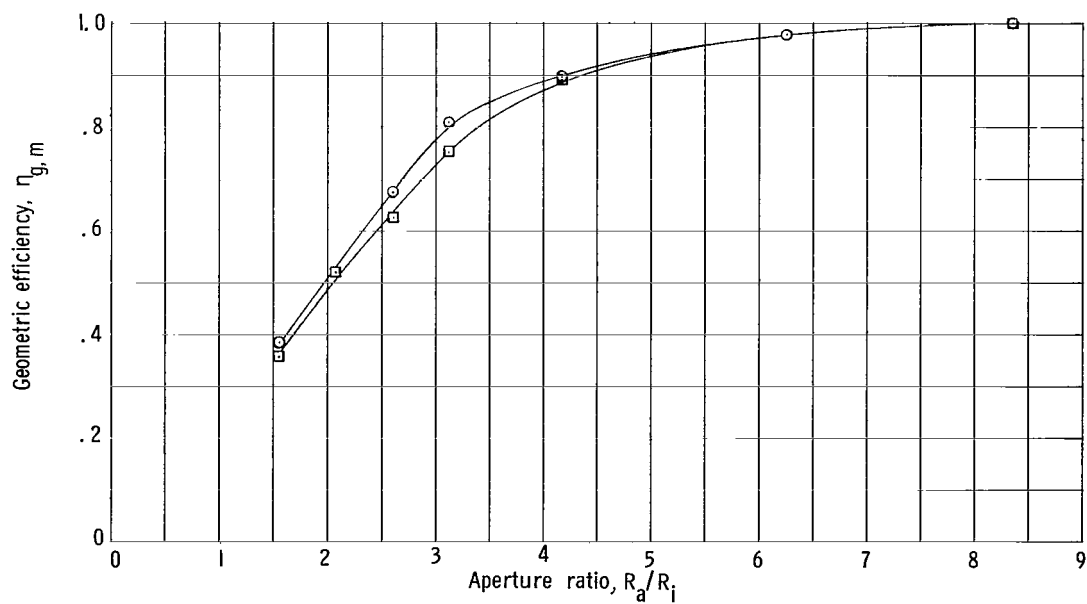


Figure 17.- Photograph showing concentrator support ring failure due to vibration testing.

L-64-3351.1



(a) Calorimetric efficiency.



(b) Geometric efficiency.

Figure 18.- Concentrator efficiency before and after vibration tests. Model 2.

050 001 28 51 3DS 68304 00903  
AIR FORCE WEAPONS LABORATORY/AFWL/  
KIRTLAND AIR FORCE BASE, NEW MEXICO 87111

ATTN: LEO RICHMAN, ACTING CHIEF TECH. LIAISON

POSTMASTER: If Undeliverable (Section 158  
Postal Manual) Do Not Return

*"The aeronautical and space activities of the United States shall be conducted so as to contribute . . . to the expansion of human knowledge of phenomena in the atmosphere and space. The Administration shall provide for the widest practicable and appropriate dissemination of information concerning its activities and the results thereof."*

—NATIONAL AERONAUTICS AND SPACE ACT OF 1958

## NASA SCIENTIFIC AND TECHNICAL PUBLICATIONS

**TECHNICAL REPORTS:** Scientific and technical information considered important, complete, and a lasting contribution to existing knowledge.

**TECHNICAL NOTES:** Information less broad in scope but nevertheless of importance as a contribution to existing knowledge.

**TECHNICAL MEMORANDUMS:** Information receiving limited distribution because of preliminary data, security classification, or other reasons.

**CONTRACTOR REPORTS:** Scientific and technical information generated under a NASA contract or grant and considered an important contribution to existing knowledge.

**TECHNICAL TRANSLATIONS:** Information published in a foreign language considered to merit NASA distribution in English.

**SPECIAL PUBLICATIONS:** Information derived from or of value to NASA activities. Publications include conference proceedings, monographs, data compilations, handbooks, sourcebooks, and special bibliographies.

**TECHNOLOGY UTILIZATION PUBLICATIONS:** Information on technology used by NASA that may be of particular interest in commercial and other non-aerospace applications. Publications include Tech Briefs, Technology Utilization Reports and Notes, and Technology Surveys.

*Details on the availability of these publications may be obtained from:*

SCIENTIFIC AND TECHNICAL INFORMATION DIVISION  
NATIONAL AERONAUTICS AND SPACE ADMINISTRATION  
Washington, D.C. 20546